Research Square

Preprints are preliminary reports that have not undergone peer review.
They should not be considered conclusive, used to inform clinical practice,
or referenced by the media as validated information.

Synthesis, Quantum Chemical Calculations, Molecular Docking and Studying the Effect of High Energetic Gamma Irradiation on Cu(I, II), Zn(II) and Cd(II) Complexes with their Antibacterial Activity.

Hussein Elganzory (hhsien@qu.edu.sa)
Qassim University College of Science https://orcid.org/0000-0002-9426-5434

Research Article

Keywords: Thiosemicarbazide, Complexes, Irradiation, DFT, X_ray, Docking, Antibacterial, Thermal.

Posted Date: August 27th, 2021

DOI: https://doi.org/10.21203/rs.3.rs-836470/v1

License: This work is licensed under a Creative Commons Attribution 4.0 International License. Read Full License

Abstract

New complexes of Cu(I,II), Zn(II) and Cd(II) of thiosemicarbazide ligand 1-(p-(methylanilinocetyl-4-phenyl-thiosemicarbazide)(H_2L_B) have been prepared and characterized by ^{1}HNMR, Mass spectra, FT-IR, elemental analyses, molar conductance, UV-visible spectra, magnetic susceptibility measurements, thermogravimetric analysis (TGA/DTG) and X-ray diffraction pattern before and after irradiation. The results confirmed that gamma ray enhanced the stability of irradiated compounds as compared to non-irradiated compounds. XRD patterns proved that increasing the crystallinity of the samples and the particles in nano range after gamma irradiation. The obtained data indicated that the Cu(I) and Cd(II) ions coordinated to the ligand through the (C = O), N(2)H and (C = S), the ligand behaves as neutral tridentate. While in complexes Cu(II) and Zn(II)complexes (B_2 and B_3) the ligand behave as neutral tetradentate and coordination take place via (C = O) and two N(2)H. These studies revealed that, two kinds of stereochemical geometries; Cu(II) and Zn(II) complexes were predicted to be octahedral, Cu(I) and Cd(II)complexes were found to be tetrahedral. The theoretical conformational structure analyses were performed using density functional theory for ligand and complexes at B3LYP functional with 6-31G(++)d,p basis set for ligand and LANL2DZ basis set for complexes. The ligand and its metal complexes have been tested for their inhibitory effect on the growth of bacteria against gram-positive (*Streptococcus pyogenes)* and gram-negative *(Escherichia coli)*. Results suggested that in case of 1µg/ml and 5µg/ml for Cu(II) and Zn(II) complexes have higher activity than other complexes. The chelation could facilitate the ability to cross the cell membrane of *E. coli* and can be explained by Tweedy's chelation theory. Molecular docking investigation proved that; the Zn(II) complex had interesting interactions with active site amino acids of topoisomerase II DNA gyrase enzymes (code: 2XCT).

1. Introduction

Thiosemicarbazones are compounds which have increased importance over the decades as prospective medicine candidates. When coordinated to elements, they have evidenced as good antitumour, antimicrobial, antioxidant and antiprotozoal managers. Transition element created complexes hold several advantages over other metal chelated because of their good acceptability and decrease toxicity in living organisms [1]. Thiosemicarbazone compound are of diverse importance for the reason that of their useful for living and pharmacological activities. Thiosemicarbazone derivatives have found application in drug development for the treatment of central nervous system disorders, of bacterial infection, as well as analgesic and antiallergic agent. Thiosemicarbazones are potent intermediates for the synthesis of pharmaceutical and bioactive materials and thus, they are used extensively in the field of medicinal chemistry. Moreover, thiosemicarbazones have found their way into almost every branch of chemistry; commercially they are used as dyes, photographic films, plastic and in textile industry [2] The biological activity of these compounds depends upon the starting materials and their reaction conditions, also related to molecular conformation in particular, which can also be significantly affected by the presence of intra- and intermolecular hydrogen bonding [3]. Thiosemicarbazones commonly performance such as chelating compound for metal ions, attachment through (C = S) and (C = N–) groups, although in several cases they behave as mono dentate compound where they bind through (C = S) only [4]. A series of copper(II) complexes of 2- phenylamino acetyl-N-phenyl hydrazine carbthioamide (H_2L) have been prepared and characterized by chemical and physical studies. The thermal behaviors of these chelates before and after γ-irradiation show that the complexes have induced more thermal stability after γ-irradiation. Solid state dc electrical conductivity for complexes was investigated before and after γ- irradiation [5, 6]. Recently, complexes of

VO^{2+}, Mn^{2+}, Zn^{2+}, Ru^{3+}, Pd^{2+}, Ag^{+} and Hg^{2+} have been prepared by reacting their metal salts with ligand, named (4-(4-chlorophenyl)-1-(2-(phenylamino) acetyl) thiosemicarbazone). Structure of synthesized metal complexes was confirmed by different analytical and spectral techniques (^{1}H NMR, MS, FT-IR, UV-Vis, EPR and Powder X-ray diffraction), thermogravimetric studies as well as molecular modeling. FT-IR spectra showed that the compound behave as neutral or monobasic tetradentate. In case of complexes of Mn^{2+}, Zn^{2+}, Ag^{+} and VO^{2+}, through (N2-H), (C = O) or (C–O) groups. X-ray diffraction pattern of Mn^{2+}, Pd^{2+} and Ag^{+} complexes before and after irradiation are recorded. XRD studies exhibited that decrease in the crystalline size of sample Mn^{2+} as compared of samples Ag^{+} and Pd^{2+} upon irradiation and irradiation influenced the crystallinity of the complexes. The possible structures of the ligand, Mn^{2+}, Pd^{2+} and Hg^{2+}complexes have been computed by means of the molecular mechanic calculations using the hyper chem. 8.03 molecular modeling program. The effect of gamma irradiation was investigated by recording the new results of pervious spectroscopic techniques and other measurements. The TGA studies of unirradiated and irradiated complexes showed that irradiated complexes were more thermally stable than unirradiated. The compound and its metal complexes have been experienced for their inhibitory outcome on the growth of microorganisms against gram positive and gram negative. The results proved that the complexes $\mathbf{B_1 - B_7}$ have potent antibacterial activity as compared to that of ligand [7–10]. In this work we described the synthesis, characterization, DFT, molecular docking as well as antibacterial activities of Cu(I,II), Zn(II) and Cd(II) of complexes of ligand 1-(p- (methylanilinocetyl-4-phenyl-thiosemicarbazide)(H_2L_B).

2. Materials And Methods

2.1. Materials

All chemicals used in this study were of analytically reagent grade, commercially available from Fulka and used without previous purification as CuI (anhydrous), $Cu(ClO_4)_2.3H_2O$, $ZnCl_2.3H_2O$ compounds which represent the metal ions used in and $CdCl_2$ (anhydrous), complexation process. All solvents were used as it is without previous purifications.

2.2. Synthesis of thiosemicarbazide ligand (H_2L_B)

The organic ligand 1-(p-(methylanilinocetyl-4-phenyl-thiosemicarbazide) (H_2L_B) was prepared by mixing equimolar amount of desired hydrazide (0.01mol) in 10 ml of absolute ethanol and the appropriate amount of phenyl isothiocynate in 10 ml of absolute EtOH. The reaction mixture was reflux for 6 hrs. After cooling, the resulting precipitate was filtered off, washed several times with ethanol and diethyl ether and dried in vacuum in presence of P_4O_{10}.

2.3. Synthesis of metal complexes

The metal complexes were prepared by adding to hot absolute ethanol solution (~ 20 mL) $MX_2.nH_2O$ where M = Cu(I and II), Zn(II), Cd(II), and X = I^{-}, ClO_4-, SO_4^{--} and Cl^{-}, $^{-}$, n = 0–1 in appropriate molar ratio. The resulting mixture was magnetically stirred at 60 ^{o}C for 6–8 h. The formed precipitate was filtered off while hot, otherwise the solution was left at 35^{o}C to evaporate some of solvent to promote crystallization. The crystals were collected by vacuum filtrations, washed several times with anhydrous diethyl ether and dried under vacuum in presence of P_4O_{10}.

2.4. Physical measurements

Elemental analyses (C, H and N) were performed at Microanalytical unit, Cairo University. Metal and halide analyses were estimated using standard literature methods [11]. The Fourier Transform Infrared (FT-IR) measurements were performed (4000–400 cm^{-1}) in KBr discs using Nenexeus-Nicolidite-640-MSA FT-IR, Thermo-Electronics Co. The UV–visible absorption spectra were measured in DMF solution using 4802 UV/vis double beam spectrophotometer. The ^{1}H-NMR spectra have been recorded in DMSO-d_6 as a solvent using Varian Gemini 200 NMR spectrophotometer and Varian-Oxford Mercury at 300 MHz, respectively.

Thermal analysis (TG/DTG) was obtained out by using a Shimadzu DTA/TG-50 Thermal Analyzer with heating rate of 10°C/min in nitrogen atmosphere with a following rate 20 mL/min in the range of ambient temperature up to 800°C using platinum crucibles. X-ray powder diffraction analyses of solid samples were measured using APD 2000 PROModel GNR-X-ray Diffractometerat (NRC, Tanta University, Egypt). X-ray diffractograms gives computer control formally finished by PHILIPS®MPDX´PERT X-ray diffratometer ready with Cu radiation CuKα (λ = 1.540 56 Å). The x´pertdiffractometer has the Bragg- Brentano geometry. The x-ray tube used was a copper tube operating at 40 kV and 30 mA. The scanning range (2θ) was 5–90° with step size of 0.050° and counting time of 2 s/step. Quartz was used as the standard material to accurate for the instrumental expansion. This identification of the complexes was done by a known method. From the fit identified Scherer formula, the average crystallite size (D) is D = (Kλ /β Cos θ)

Where: λ is the X- ray wavelength in the nanometer, K is factor related to crystallite shape, and with a value about 0.9 and ß is the peak width at half maximum height. The value of ß in the 2θ axis of diffraction shape must be in radians. The θ is the Bragg angle and be able to in radians since the Cos θ compatible with the same number.

2.5. Computational studies

The input files of ligand and its metal complexes were prepared with GaussView 5.0.8 [12] Gaussian 09 rev. A.02 [13] was used to make the all calculations by the DFT/B3LYP method. 6-31G (++)d, p and LANL2DZ are the standard basis sets for the synthesized ligand and its metal complexes, respectively.

2.6. Irradiation studies

For irradiation studies of solid samples of ligand and complexes were subjected to **γ**-irradiation [14] to a dose of 60 kGy using Indian ^{60}Co γ-ray cell type GE-4000 A (at room temperature at the Egyptian Atomic Energy Authority Nasr City, Egypt) at a dose rate of 2.2 kGy h^{-1}. After removing the samples from the radiation field the FT-IR, absorption spectra ,XRD and thermal analysis (TG/DTG) and biological activity of the irradiated samples were investigated by the same methods used for before irradiated compound **.**

2.7. Antibacterial activity

The *in vitro* antibacterial activity studies were carried out at Genetic Engineering and Biotechnology Research Institute, Department of Microbial Biotechnology at Sadat City University, Egypt, by using Broth Dilution Method [15, 16] with some alterations, to investigate the inhibitory effect of some synthesized complexes before (**B_1-B_4**) and after (**A_1-A_4**) irradiation on the sensitive organisms *Streptococcus pyogenes* as Gram- positive bacteria and *Escherichia coli* as Gram–negative bacteria. Nutrient broth medium was prepared by using Brain Heart Infusion (BHI) broth and distilled water. The test compounds in measured quantities were dissolved in DMSO which has

no inhibition activity to get two different concentrations (1mg/mL, 5mg/mL) of compounds. The strains selected for the study were prepared in (BHI) broth medium with shaking and autoclaved for 20 min 15 pounds of pressure and at 121 ^{o}C before inoculation. The bacteria were then cultured for 24 h at 37 ^{o}C in an incubator.. One ml of the standard bacterial culture was used as inoculation in a nutrient broth. For growth studies, culture of microbial cells were inoculated and grown aerobically in BHI broth for control and along with various concentrations of the test compounds in individual flasks. Growth was calculated turbidometrically at 650 nm using conventional Spectrophotometer, in which turbidity produced is measured by taking absorbance and compared with turbidity produced by control. The growth rate of different bacteria in absence as well as in presence of test compounds was performed for each concentration. Absorption measurements were accomplished by spectrophotometer after 24 and 48 h of incubation to determine the number of viable organisms per milliliter of sample and were used to the calculated the % inhibition.

3.8 Molecular docking

All docking steps were done by MOE 2008 (Molecular Operating Environment) software to simulate the binding model of these compounds into topoisomerase II DNA gyrase enzymes (2XCT). The protein crystal structure was obtained from the Protein Data Bank (PDB).

3. Results And Discussion

3.1. Elemental analysis and molar conductance

The analytical and physical data of the prepared ligand and metal complexes are collected in **Table (1)**. The chemical composition and stoichiometry of the prepared metal complexes were confirmed by the results of elemental analysis. The obtained data showed satisfactory agreement with the proposed molecular formulae. These data also indicated that the metal complexes have 1:1 (metal: ligand) stoichiometry.

The complexes are found to be air stable for a long time, insoluble in different organic solvents such as (ethanol, methanol, carbon tetrachloride, chloroform, dichloromethane and acetone) but soluble to great extent in DMF and DMSO. Conductivity measurements in non-aqueous solution have frequently been used in structural studies of the prepared metal complexes within the limits of their solubility. The molar conductance values of 10^{-3} M solution of the complexes in DMF are listed in **Table (1)** show that copper complexes(B1 and B2) are non-electrolytes in nature [17]. However, complexes (B_3, B_4) show molar conductivity values of 72 and 65 ohm^{-1} cm^2 mol^{-1} indicating 1:2 and 1:1 electrolytic nature in DMF(10^{-3} mol L^{-1}) solution, respectively [18].

Table 1
Elemental analyses and physical properties of ligand (H2LB) and its metal complexes.

No.	Molecular formula	(Emperical formulae)	M.wt.	Colour (Yield %)	C	H	N	M	Λ_m
	H_2L_B	($C_{16}H_{18}N_4OS$)	314	Buff 75	61.1 (61.3)	5.73 (5.70)	17.8 (17.9)	-	-
B_1	$Cu(H_2L)I$	($C_{16}H_{18}N_4OSICu$)	504.5	Green 78	38.1 (38.4)	3.6 (4.2)	11.1 (11.4)	12.6 (12.3)	25
B_2	$Cu(H_2L)_2(ClO_4)_2$	($C_{32}H_{36}N_8O_{10}S_2Cl_2$ Cu)	889.5	Green 60	43.2 (43.8)	4.0 (3.78)	12.6 (12.9)	7.1 (7.6)	24
B_3	[Zn $(H_2L)_2(H_2O)]SO_4$	($C_{32}H_{38}N_8O_7S_2$ Zn)	807.4	Yellow 65	47.5 (47.2)	4.7 (4.9)	13.8 (13.6)	8.1 (8.3)	72
B_4	[Cd (H_2L)Cl]Cl	($C_{16}H_{18}N_4OSCl_2Cd$)	497.4	White 70	38.6 (39.2)	3.6 (4.3)	11.3 (11.5)	22.6 (23.0)	65

Λ_m = molar conductivity (ohm^{-1} cm^2 mol^{-1}) in 10^{-3} M DMF solution

3.2. Nuclear magnetic resonance spectroscopy

The ^1H NMR is a helpful tool for the preparation of organic compounds in conjugation with other spectrometric information, nuclear magnetic resonance is a physical phenomenon based upon the magnetic properties of an atom's nucleus.. The most commonly used nuclei are hydrogen[l] and carbon[13], although certain isotopes of many other elements nuclei can also be observed. Comparison of the proton nuclear magnetic resonance of 1-(p-(methylanilinocetyl-4-phenyl-thiosemicarbazide) ligand before and after γ- irradiation (H_2L_B and H_2L_A) recorded in DMSO-d_6 solution is found in (Fig. 1). The ^1H NMR spectrum of the ligand before γ - irradiation(H_2L_B) in DMSO-d_6 exhibited a chemical shift (δ \ppm) = 2.5ppm for (DMSO) before and after γ- irradiation, the N(4)H signal appears with 9.44 ppm and the N(2)H signal appears with 9.51, 10.05 ppm indicating the involvement of these hydrogen through intra-molecular hydrogen bonding with the carbonyl oxygen, the peak of N(1)H appeared at 9.62 ppm for ligand after gamma irradiation .The singlet signal appears with 2.14, 3.9, 3.7 ppm attributed to the protons of methyl CH_3, singlet signal appears with 3.7 ppm attributed to the protons of CH_2, the multiplet signal appears with 5.85–7.1, 6.5–7.4 ppm attributed to the aryl protons. The intensity of the bands after irradiation are higher than before irradiation and some bands disappear upon irradiation [19, 20].Also ^1H NMR spectra of [$Zn(H_2L)_2$ SO_4] before and after γ-irradiation (B_3,A_3) displayed signals at 2.14(s, 6H, $2CH_3$), 3.76(s,4H,$2CH_2$), 5.59(s,2H,2NH), 6.32–7.43(m, 18H, Ar-H), 9.55(s,1H, NH) and10.51(s, H, NH) as shown in (Fig. 2) and. While [$Cd(H_2L)Cl_2$] before and after γ-irradiation (B_4, A_4) complexes displayed signals at 2.16(s, H, CH_3), 3.77(s,2H,$2CH_2$), 5.56(s, H, NH), 6.51–7.52(m, 9H, Ar-H), 9.44 (s,1H, NH), 9.61 (s,1H, NH) and 10.05(s, H, NH) as shown in Fig. 3.

The effect of γ-irradiation on the chemical shift of $[Zn(H_2L)_2]SO_4$ and $[Cd(H_2L)Cl]Cl$ after γ-irradiation are similar to before irradiation.

3.3. Mass spectroscopy

Mass spectral data confirm the structure of the ligand as indicated by the molecular ion peak (M^+) corresponding to their molecular weight. MS of H_2L_B (**Fig. 4)** confirms the proposed formula, the observed peak at *m/z* = 313*amu* (M) corresponding to the ligand moiety ($C_{16}H_{18}N_4OS$, atomic mass *m/z* = 314 molecular ion peak). The spectrum also shows important fragment ions in the range *m/z* = 51 for $[C_4H_4\text{-}H]^+$, 77 for $[C_6H_5]^+$, 107 for $[C_7H_8N]^+$ base peak, 120 for $[C_7H_6NO]^+$, 135 for $[C_8H_7S]^+$, 280 for$[C_{14}H_{13}N_3SO\text{-}H]^+$ and 313 for$[C_{16}H_{18}N_4SO\text{-}H]^+$may be assigned to different fragments.

Also the spectrum of complex (B_3) confirms the proposed formula by showing a molecular ion peak at m/z 807.4 amu corresponding to $[Zn(H_2L)_2(H_2O)SO_4]$ (B_3) (Fig. 5) which coincide with its formula weight (calculated m/z = 807.4 amu). The other fragments of the complex give the peak with various intensities at different m/z values like at Calc/Found: 77 $[C_6H_5]$, 91 $[C_6H_4NH]$, 120$[C_9H_8NH]$, 255 $[C_{13}H_{13}N_5O]$, 535$[C_{24}H_{24}N_8O_2]$, 715$[C_{30}H_{29}N_8O_4S_2]$, 783$[C_{30}H_{38}N_8O_7S_2Zn]$, 807.4/806 $[C_{32}H_{38}N_8O_7S_2\ Zn]$.

3. 4. Ft-ir Spectra

3.4.1. FT- IR spectra of the ligand before and after γ-irradiation

The comparison between the functional groups of the ligand before and after irradiation (H_2L_B and H_2L_A) the infrared spectra are presented in Fig. 6 and Table 2. It has been found that the functional groups of the ligand before γ-irradiation and after presented at 3384,3336 cm^{-1}; 3263,3185cm^{-1}; 3150,3126cm^{-1}; 1672,1689 cm^{-1} and 749,750 cm^{-1} are attributed to the stretching frequencies of υ(N4-H), υ(N2-H) and υ(N1-H), υ(C = O) and υ(C = S) respectively. After γ-irradiation the bands corresponding to υ(C = O) shift to higher frequencies or slightly shift as compared with before γ-irradiation [21]. After γ-irradiation the intensity of the peaks are more sharper than before γ-irradiation.

Table 2

Infrared spectral bands (cm^{-1}) for ligand and its metal complexes before and after irradiation

No	Compound	υ (OH)/ υ (N4-H)	υ (N2-H)	υ (N1-H)	υ (C = O)	υ (C = S)	υ (M-O)	υ (M-N)
	H_2L_B	3384	3263	3150	1672	749	-	-
	H_2L_A	3336	3185	3126	1689	750		
B_1	$Cu(H_2L)I$	3431	3293	3183 3150	1597	749	603	529
A_1	$Cu(H_2L)I$	3434	3295	3185 3151	1597	750	602	529
B_2	$Cu(H_2L)_2\ (ClO_4)_2$	3437	3295 3206	3153 3122	1595	754	614	545
A_2	$Cu(H_2L)_2(ClO_4)_2$	3433	3297 3209	3154	1595	756	612	539
B_3	$[Zn\ (H_2L)_2(H_2O)]SO_4$	3420	-	3170	1593	754	614	512
A_3	$[Zn\ (H_2L)_2(H_2O)]SO_4$	3420 3277	-	3138 3164	1619 1593	755	618	512
B_4	$[Cd(H_2L)\ Cl]\ Cl$	3426	3268	3179	1685 1613	744	591	533
A_4	$[Cd(H_2L)Cl]\ Cl$	3433	3269	3179	1685 1617	744	591	532

Where: B = before γ-irradiation, **A =** after γ-irradiation

3.4.2. FT-IR spectra of copper complexes before and after γ-irradiation

The FT-IR spectra of the Cu(I, II) complexes before and after γ-irradiation (B_1, B_2 and A_1, A_2) show significant changes compared to the spectrum of the free ligand (Figs. 7 and 8). The most important diagnostic spectral bands are summarized in Table 2. The IR spectra of copper complexes (B_1, B_2 and A_1, A_2) show strong bands at 3431; 3437; 3293; 3295; 1597; 1595 and 749; 754 cm^{-1} for before irradiation, also at 3434; 3433; 3295; 3297; 1597; 1595 and 750;756 cm^{-1} for after irradiation which assigned to the stretching frequencies of υ(N4-H), υ(N2-H), υ(C = O) and υ(C = S). The bands corresponding to υ(N4-H), υ(N2-H), υ(C = O) and υ(C = S) appear at the same frequency or slightly shift to higher frequency after gamma irradiation. The IR spectra of Cu complexes before irradiation show that υ(C = O) and υ(N2-H) shift to lower frequency upon complexation as compared of free

ligand, indicating that coordination of the ligand in keto-form and the ligand behaves as neutral bidentate or tetradentate, coordination take place via (C = O) and N(2)H.

The IR spectra of Cu(I, II) complexes before and after γ- irradiation display new bands at 603, 614 and 529,545 cm^{-1} assigned to υ(Cu-O) and υ(Cu-N) respectively [22, 23]. IR spectra of the complexes (A_1 and A2) showed that the intensity of the IR bands became more intense than before γ- irradiation [24].

3.4.3. IR spectra of Zinc(II) complexes before and after γ-irradiation

The IR spectra of Zn(II) complexes (Fig. 9) show strong bands at 3420,3170, 3164, 1593, 1619 and 754,755 cm^{-1} before irradiation and after γ-irradiation which attributed to the stretching frequencies of υ(N4-H) υ(N1-H), υ(N2-H), υ(C = O) and υ(C = S)wagging vibrations, respectively. The IR spectra of Zn(II) complex before and after γ-irradiation it is seen that the band corresponding to υ(C = O) was shifted to lower frequency upon complexation and the ligand behave as neutral tetradentate and coordination take place via two (C = O) and two (N2-H), the band corresponding to υ(N4-H) appears at the same frequency for before γ- irradiation and after γ-irradiation, high intensity of the bands of function groups after γ-irradiation. The new bands appeared at 614,618 and 512 cm^{-1} are assigned to υ(Zn-O) and υ(Zn-N), respectively [25].

3.4.4. FT-IR spectra of Cd(II) complexes before and after γ-irradiation

The FT-IR spectra of Cd(II) complexes (Fig. 10) show strong bands at 3426, 3433; 3268, 3269; 3179; 1685 and 744 cm^{-1} before irradiation and after γ-irradiation which attributed to the stretching frequencies of υ(N4-H) υ(N2-H), υ(N1-H) and υ(C = S)wagging vibrations, respectively. The IR spectra of Cd(II) complexes before and after γ-irradiation showed that the band corresponding to υ(C = O) is shifted to higher frequency upon complex formation and the ligand behave as neutral tridentate and coordination take place via (C = O), (N2-H) and (C = S), the band corresponding to υ(N4-H) shifts to higher frequency after γ-irradiation, high intensity of the bands of function groups after γ-irradiation. The new bands appeared at 591and 533, 532 cm^{-1} assigned to υ(Cd-O) and υ(Cd-N) respectively [26].

3.5. UV- Vis spectra and magnetic moment properties

The electronic spectral bands of the ligand (H_2L_B) and Cu(I, II), Zn(II) and Cd(II) complexes in DMF solution within the range 200–800 nm are tabulated in Table 3 and depicted in Figs. (11–14). The electronic spectrum of the ligand exhibits bands at 314, 292 and 279 nm, respectively.

3.5.1. The electronic absorption spectra of copper complexes before and after γ- irradiation.

The electronic spectra of Cu(I) complexes before and after irradiation (B_1 and A_1) display bands at 300 and 409 nm, respectively. Cu(I) ions have the d^{10} configuration and therefor the Cu(I) complexes should not exhibit any d-d transition and have tetrahedral geometry [27].

While the electronic absorption spectra of Cu(II) (B_2 and A_2) before and after irradiation exhibited bands at 308, 398 and 653 nm in DMF refer to L→M charge transfer and d→d transitions, respectively in octahedral geometry [28]. Diamagnetic behavior of complex (B_1) and the magnetic suitability value of complex (B2) is 1.78 B.M., which is an indicative of tetrahedral and octahedral geometry [27, 29].

3.5.2. Zinc(II) complexes before and after γ-irradiation

The electronic absorption spectra of Zn(II) complexes before and after γ-irradiation displayed bands at 300, 282; 448 and nm in DMF solution, octahedral structure of Zn(II) complex is suggested which is diamagnetic in nature [30].

4.5.3. Cadium(II) complexes before and after γ-irradiation

The electronic absorption spectra of Cd(II) complexes before and after γ-irradiation displayed three bands at 284,390, 610 nm ; 282,385and 608 nm in DMF solution attributed to charge transfer transition which assigned to tetrahedral geometry around Cd(II) ion [31, 32]. The Cd(II) complexes are diamagnetic because of d^{10} electronic configuration of Cd(II) ion [33].

Table (3). The electronic absorption spectral data in DMF solution of ligand and its magnetic moment and metal complexes before and after irradiation value

No	Compound	Assignment		
		DMF	μ_{eff} (B.M.)	Geometry
	H_2L_B	314, 292, 279	-	L
B_1	$Cu(H_2L)I$	300 409	Dia	Tetrahedral
A_1	$Cu(H_2L)I$	300 408	Dia	Tetrahedral
B_2	$Cu(H_2L)_2(ClO_4)_2$	653 398 308	1.74	Octahedral
A_2	$Cu(H_2L)_2(ClO_4)_2$	653 398 308	-	Octahedral
B_3	$[Zn\ (H_2L)_2(H_2O)]SO_4$	448 300	Dia	Octahedral
A_3	$[Zn\ (H_2L)_2(H_2O)]SO_4$	445 282	Dia.	Octahedral
B_4	$[Cd\ (H_2L)Cl]Cl$	610 390 284	Dia.	Tetrahedral
A_4	$[Cd\ (H_2L)Cl]Cl$	608 385 282	Dia.	Tetrahedral

3.6. X-ray diffraction patterns

XRD analysis was performed to confirm the crystal phase of compound. Samples B_1-B_3 and A_2,A_3 (was just before and after the irradiation as shown in Figs. 15–17 and Table (4). The XRD patterns of the synthesized compounds were carried out in order to give an insight about the lattice dynamics of the compounds. The X-ray diffraction were recorded by using ($Cu_{K\alpha}$) radiation (1.5406 Å). The intensity were collected over a 2h range of 5–90^o. The average grain size of the samples was estimated using the diffraction intensity peak. The pattern found reflects a tracker on the fact that each solid describes a definite compound of a definite construction which is not contaminated with initial materials. This identification of the complexes was done by a known method [34].The

mean grain size (D) of the particles was determined from the XRD line broadening measurement using the Scherrer equation: $D = 0.89\lambda/\beta\ (Cos\theta)$

An observable peak sharpness in the diffraction pattern indicates that the Cu(I, II) and Zn(II) complexes before and after irradiation (Figs. 15–17 and Table (4) are in the nanometer range. The diameter of particles are found in nanorange scale as follows: Cu(I) complex before (B_1) 4.83nm; Cu(II)complexes before and after irradiation(B_2 and A_2) 3.6, 5.79 nm; Zn(II) complexes before and after irradiation (B_3 and A_3) 5.97, 3.84 nm. The nanoparticles sized complexes may serve strongly in different application fields in between the biological one [35].

Figures (15–17) show that Cu(I,II), Zn(II) complexes new peaks appear and some peaks displaced to longer interplanar spacings. The major factors tending to influence the intensity of powder patterns are structure factor, polarization factor, atomic scattering factor, multiplicities and preferred orientations. Upon irradiation, the position of atoms in the lattice changes and consequently, the scattering power also changes, leading to changes in intensity which display high resistance [36]. It should be noted that the Zn(II) complex (A_3) after irradiation increases the crystalline size than B_3 before irradiation.

Table 4. XRD data of Cu(I, II) , Zn(II) complexes before (B_1, B_2, B_3) and after irradiation(A_2,A_3)

B_1			
8.2714	10.68097	0.36400	3.84
21.1130	4.20458	0.42670	3.47
23.6719	3.75554	0.34640	4.36
25.3735	3.50741	0.31710	4.83
42.0811	2.14551	0.28810	6.47
49.08440	1.82802	0.31140	6.78

A_2			
8.2002	10.77355	0.29380	4.75
23.6566	3.75794	0.40670	3.71
25.3683	3.50812	0.26470	5.79
28.2666	3.15466	0.29330	5.36
42.0890	2.14513	0.24600	7.59
49.8356	1.82831	0.21410	10.03

B_2			
5.4796	16.11496	0.32540	4.27
6.6475	13.28611	0.39730	3.51
8.7388	10.11071	0.38950	3.6
21.9376	4.04836	0.81600	1.83
23.5451	3.77548	0.52750	2.86
26.7430	3.33083	0.4900	3.16

A_3			
6.6293	13.32254	0.36300	3.84
12.0777	7.32205	0.23540	6.02
13.4246	6.59030	0.26640	5.34
19.1065	4.64136	0.23490	6.24
20.0901	4.41629	0.26420	5.58
21.01650	4.19437	0.21000	7.07

B_3			
6.6762	13.22906	0.23340	5.97
11.1930	7.89872	0.24200	5.83
12.1177	7.29797	0.26890	5.27
13.4750	6.56576	0.24240	5.87
19.1602	4.62848	0.22050	6.65
20.1275	4.40817	0.26500	5.57

3.7. Thermal behavior of ligand and metal complexes before and after γ-irradiation

The thermal behavior of the ligand and Cu(I, II), Zn(II) and Cd(II) complexes before and after γ-irradiation was investigated by thermogravimetric technique in temperature range 25–800°C. The thermal behavior data of the ligand and Cu(I,II), Zn(II) and Cd(II) complexes (B_1, B_2, B_3, B_4 and A_1 ,A_2, A_3, A_4) before and after γ-irradiation are tabulated in Table 5 and depicted in Figs. (18–20).

3.7.1. The ligand before and after γ –irradiation

The TG curves of the ligand before and after γ-irradiation show that it is thermally stable till 140°C,125°C, respectively. Also the TG curves show three decomposition steps in the temperature range 140–550 ^{o}C ;125–510°C with total weight loss of Calc.100% (Found 100%) before and after γ-irradiation, respectively.

3.7.2. Copper Complexes

The TG thermograms of copper complexes (B_1 and A_1) display three steps of decomposition as shown in Table 5 and Fig. (18). The first step of decomposition appeared within the temperature range 134–255 and 147–293 °C with mass loss of 21% (calc. 21.2%) and 28.7% (calc. 28.3%) for complex (B_1) and complex (A_1), respectively, corresponding to loss of ($CH_3C_6H_5NH$) and (HI + NH). The second step appeared at 258–410 and 294–385°C with mass loss of 19.0% (calc. 18.2%) and 11.0% (calc. 10.1%) for complexes (B_1 and A_1), respectively, corresponding to further decompositions of organic ligand. The third TG decomposition step appeared within the temperature ranges 410–753°C and 385–701°C with mass loss of 36.0% (calc. 36.5%) and 35.0% (calc.34.1%), respectively, corresponding to complete decomposition of the organic ligand. The final remained product appeared above 735°C with remain mass of 24.0% (calc. 22.9%) for complex (B_1) and above 701 °C with mass remain of 25.3% (calc. 25.3%) for complex(A_1) represent the formation of (CuO + 3C) and (CuO + 4C) as a final product [37].

The TGA curve of copper complexes (B_2 and A_2) display successive steps of decomposition as shown in Table 5 and Fig.(S1). The decomposition starts within the temperature range 420–620 and 440–790°C with mass loss of 82.0% (calc. 83%) and 84.4% (calc. 84.6%) for complex (B_2) and complex (A_2), respectively. The final thermoproduct appeared at 620°C with mass loss 18.0% (calc. 17%) for complex (B_2) and at 790 °C with mass loss 15.6% (calc. 15.7%) for complex(A_2) represents the formation of (CuO + 7C) and (CuO + 6 C) as a final product [37].

3.7.3. Zinc (II) Complex

The TG thermograms of Zn(II) complexes (B_3,A_3) showed several steps of decomposition. The first step of decomposition appeared at 180–332 and 170–354°C with mass loss 39% (calc. 39.3%) and 50% (calc. 50.3%) for complexes B_3 and A_3 which corresponded to decomposition of organic ligand. The second step of decomposition appeared at 332–749 and 354–705°C with mass loss 39% (calc. 38.8%) and 50% (Calc.50 %)), respectively, for complexes (B_3,A_3) which attributed to complete decomposition of organic ligand. The remaining weigh for complex (B_3) appeared above 704°C and above 660°C with mass remain of 22.1% (calc. 21%) and 21% (calc. 21.7%)corresponding to the formation of ZnO as final products in addition to 7C residue [37].

3.7.4. Cadmium (II) Complexes

The TG thermograms of Cd(II) complexes (B_4, A_4) display successive decomposition steps within the temperature range 134–789 and 139–718°C with mass loss 88.2% (calc. 88.5%), respectively for complexes (B_4, A_4), are assigned to the material decomposition. The final weight residue appeared at above 789 and 718°C corresponded to Cd and CdO for complexes (B_4,A_4) as thermo finial products in addition to carbon residue for complex (A_4) [38].

Table 5
Thermal analysis data of ligand and Cu(I, II), Zn(II) and Cd(II) complexes before and after irradiaton

No.	Molecular formulae	Temp. range (°C)	Temp. range (°C)	Mass loss %		Assignment
		DTG	TGA	Found	Calc.	
	H_2L_B	180,500	140	-	-	Melting Decomposition
			140–550	100	100	
	H_2L_A	180,550	125	-	-	Melting Decomposition
			125–510	100	100	
B_1	$Cu(H_2L)I$	206	134–255	21	21.2	Loss of $CH_3C_6H_5NH$
		313	255–410	19.0	18.2	Further Decomposition
		639	410–753	36.0	36.5	Completion of decomposition of organic ligand
				24	22.9	CuO + 3C
A_1	$Cu(H_2L)I$	287	147–293	28.7	28.3	Loss of $CH_3C_6H_5NH$ + HI + NH
		314	294–385	11	10.1	Further Decomposition
		602	385–701	35	34.1	Complete Decomposition
				25.3	25.3	of organic ligand
						CuO + 4C
B_2	$Cu(H_2L)_2(ClO_4)_2$	547, 637, 685	420–620	82	83	Decomposition
			at 620	18	17	CuO + 7C as final product
A_2	$Cu(H_2L)_2(ClO_4)_2$	429	440–790	84.4	84.3	Decomposition
			at 790	15.6	15.7	CuO + 6C as final product
B_3	$Zn(H_2L)_2(H_2O)SO_4$	216	180–332	39	39.3	decomposition
		384	332–499	39	38.8	Complete decomposition of the organic ligand
		646	499–704	22	21	ZnO_2 + 7C
A_3	$Zn(H_2L)_2(H_2O)SO_4$	220	170–374	50	50.3	Decomposition
		599	374–660	29	28	Complete decomposition of the organic ligand
			At 660	21	21.7	ZnO_2 + 7C

No.	Molecular formulae	Temp. range (°C)	Temp. range (°C)	Mass loss %		Assignment
		DTG	TGA	Found	Calc.	
B_4	$Cd(H_2L)Cl_2$	186	134–789	88.2	88.4	decomposition
		257	At 789	11.8	11.6	Complete decomposition of the organic ligand
		335				Cd
		701				
A_4	$Cd(H_2L)Cl_2$	186	139–718	82.7	82.3	decomposition
		331	at 718	17.3	46.6	Complete decomposition proccess
		644			17.7	CdO + 2C

From all of the above, the suggested chemical structure of metal complexes are shown in Scheme 1

3.8. Structure characterization with DFT study

The geometric structures of H_2L_B ligand and its metal complexes were optimized as shown in (Fig. 21). Upon coordination of H_2L_B to the metal atom, some bond lengths become slightly longer than in the free ligand accompanied with changes in angles that were clarified in Table 6 as (C5-O8), (N4-C5), (N7-C6) and (N3-C2). This finding is due to the formation of M-N & M-O bonds in all complexes that make the C-O (S. S. Hassan, 2017, S. S. Hassan, 2018) and C-N bonds weaker (Safaa S. Hassan, 2020). It was observed from the energy values that the stability of ligand increases upon complexation with Zn (II) and Cu(II) ions in ratio (1 to 2) metal to ligand. The ionic complexes (Cd(II) & and Cu(I)) show higher energy values than the parent ligand. The polarity of ligand increased after complexation by its coordination to metal ions as it is evident from the magnitude of their dipole moments. The ionic complexes have higher polarity than the non-electrolytic complexes. The molecular properties are mentioned in Table 6 which can be calculated as follows: Hardness η = (I-A)/2, Softness (S) S = 1/2η, Chemical potential (μ), μ = -(I + A)/2 and Electronegativity (χ), χ = (I + A)/2η. From HOMO-LUMO gap (ΔE), one can detect whether the molecule is hard or soft. Larger ΔE corresponding to harder molecule and small one related to the softer molecule. The polarizability of the soft molecule is more than the hard one because it needs lower energy to excitation, thus softness (S) and hardness (η) are properties of molecule that measures the chemical reactivity. We found the ligand and Cu(I) complex were more harder than the remaining complexes. The generated molecular orbital energy diagrams HOMO and LUMO are presented in (Fig. 22).

The formal charge of cadmium, zinc and copper were Cd^{2+}, Zn^{2+}, Cu^{2+}, Cu^{+} but the calculated charges on [Cd$(H_2L)Cl]Cl$, $Cu(H_2L)_2(ClO_4)_2$, $Cu(H_2L)I$ and $Zn(H_2L)_2(H_2O)$ SO_4were 0.856, 0.579, 0.413 and 0.884, respectively. It

can be explained due to the charge transfer from the examined ligand to the central metal ions i.e. L→M. So, the theoretical calculations confirm the results that obtained from the analysis tools which were discussed in the previous characterization part.

Table 6
Ground state properties of H_2L ligand using B3LYP/6-31G(++)d,p and its metal complexes using B3LYP/LANL2DZ

Parameter	H_2L_B	$[Cu(H_2L)I]$	$[Cu(H_2L)_2(ClO_4)_2]$	$[[Zn(H_2L)_2(H_2O)]SO_4$	$[Cd(H_2L)Cl]Cl$
E_T, Hartree	-1312.9304	-1135.3041	-2676.2810	-1991.3548	-986.9751
E_{HOMO}, eV	-5.22	-6.06	-6.04	-2.52	-9.06
E_{LUMO}, eV	-1.38	-3.88	-4.91	-1.72	-8.46
ΔE, eV	3.84	2.18	1.13	0.80	0.6
I=- E_{HOMO}, eV	5.22	6.06	6.04	2.52	9.06
A= - E_{LUMO}, eV	1.38	3.88	4.91	1.72	8.46
χ, eV	3.30	4.97	5.47	2.12	8.76
η, eV	1.92	1.09	0.565	0.4	0.30
S, eV^{-1}	0.26	0.45	0.88	1.25	1.67
μ, eV	-3.30	-4.97	-5.47	-2.12	-8.76
Dipole Moment	3.2200	15.1634	3.2461	8.2389	15.7912

[a] **E**: the total energy (a.u.), [b] HOMO: highest occupied molecular orbital (eV) and [c] LUMO: lowest unoccupied molecular orbital (eV), $\Delta E = E_{lumo} - E_{Homo}$

Table 7
Some of the optimized bond lengths, Å and bond angles, degrees, for (H_2L) and complexes using B3LYP/6-311G(++)d,p.

Bond length (A°)	H_2LB	$[Cu(H_2L)I]$	$[Cu(H_2L)_2(ClO_{4)2}]$	$[Zn\ (H_2L)_2(H_2O)]SO_4$	$[Cd(H_2L)Cl]Cl$
R(M-Cl)	—	2.19937	—	—	2.37881
R(M-O8)	—	2.22007	1.93603	2.06440	2.36369
R(M-N3)	—	1.96135	2.65910	2.04013	1.94974
R(M-O-ClO_3)	—	—	1.97195	—	3.04748
R(M-S1)	—	2.60876	—	2.37828	—
R(M-O-H_2)	—	—	—	2.10239	—
R(C2-S1)	1.73273	1.80438	—	1.80719	1.46624
R(C5-O8)	1.25861	1.27510	1.27514	1.30843	1.45986
R(N4-C5)	1.35538	1.36229	1.34735	1.39788	1.32019
R(N3-C2)	1.36138	1.32646	1.46312	1.47620	1.35331
R(N7-C6)	1.44027	1.45935	1.45631	1.47188	1.45929
R(N9-C2)	1.37062	1.37303	1.34881	1.42723	1.36423
A(N3-M-Cl1)	—	175.483	—	—	68.909
A(Cl1-M-Cl2)	—	—	—	—	—
A(Cl1-M-O8)	—	108.139	—	—	118.508
A(O8-M-N3)	—	76.143	71.994	80.528	68.909
A(M-N3-N4)	—	118.525	98.360	103.377	118.280
A(M-O8-C2)	—	110.583	125.403	111.998	116.580
A(N3-M-O-ClO3)	—	—	98.448	—	—
A(O8-M- O-H_2)	—	—	—	90.905	—
A(N3-M-S1)	—	66.774	—	81.522	—

3.9. Antibacterial Activity

The synthesized ligand and its metal complexes were separately exposed to gamma irradiation to test their improvement as active antibacterial drugs [39]. Results in Table (8), Figs. 23 and 24 showed antibacterial activity against the tested microbes. Generally, it was found that antibacterial activity of both the synthetic ligand and metal complexes before and after γ-irradiation was proportionally increased with increased concentration. The tested compounds before and after γ-irradiation are found to have remarkable biological activity. The results in Table (8) Figs. (23 and 24) indicate that in case of *E.coli* for 1µg/ml and 5µg\ml the corresponding Cu(II) and

Zn(II) complexes showed much better antibacterial activity with respect to the individual ligand and complexes against the same microorganism under identical experimental conditions, the antibacterial activity of the tested compounds were found to follow the order: $A_2 > A_3 > B_1 > A_1 > B_3 > B_2 > A_4 > H_2L_A > H_2L_B > B_4$ for 1µg\ml before and after irradiation, Antibacterial activity of 5µg/ml concentration in case of *E.coli* follow the order $A_3 > B_1 > A_2 > B_3 > A_1 > H_2L_A > H_2L_B > A_4 > B_4$ before and after irradiation. On the other hand, antibacterial activity was recorded when using the ligand and metal complexes with *S.pyogenes* follow the order: $A_3 > A_2 > A_1 > B_3 > A_4 > H_2L_A > H_2L_B > B_4 > B_2 > B_1$ for before and after irradiation with1µg/ml concentration [23]. Antibacterial activity of 5µg/ml concentration for both the free acyclic ligand and its complexes before and after irradiation followed the order: $B_2 = B_3 > H_2L_A > A_2 > A_1 > A_3 > H_2L_B > B_1$ when compounds were used with *S. pyogenes* [40]. Results suggested that in case of 1µg/ml and 5µg/ml Cu(II) and Zn(II) complexes have higher activity than other complexes The chelation could facilitate the ability to cross the cell membrane of *E. coli* and can be explained by Tweedy's chelation theory. Chelation/complexation could enhance the lipophilic nature of the central metal atom which in turn, favors its permeation through the lipoid layer of the membrane thus causing the metal complex to cross the bacterial membrane more effectively thus increasing the activity of the complexes. Besides from this many other factors such as solubility, dipole moment, conductivity influenced by metal ion may be possible reasons for remarkable antibacterial activities of these complexes [41]. Exposure to gamma irradiation remarkably enhanced the antibacterial activity for both the ligand and its complexes when it was used in case of *E.coli*. The activity also increased after irradiation in case of *S. pyogenes*. This may be attributed to the different nature of the cell wall for both microbes which may be correlated with other factors such as solubility, dipole moment, and conductivity influenced by metal ion. Additionally, exposure to gamma irradiation increased the antibacterial activity of both the free a cyclic ligand and their complexes when used with both concentrations (1µg/ml and 5µg/ml) in case of the Gram positive *S. pyogenes* bacterium. It also has been observed that some moieties such as N(2)H linkage introduced into such compounds exhibits extensive biological that may be responsible for increase in hydrophobic character and liposolubility of the molecules in crossing the cell membrane of the microorganism and enhance biological utilization ratio and activity of complexes activity [42]. The antibacterial studies of the prepared compounds screened against both Gram positive and Gram negative bacteria proved that these compounds exhibit remarkable antibacterial activity and can be used in the future as therapeutic drugs for pathogenic bacterial diseases.

Table 8
Antibacterial activity of ligand and their metal complexes

No.	Compound	Inhibition %			
		S. pyogenes		E.coli	
		1µg/ml	5µg/ml	1µg/ml	5µg/ml
	H_2L_B	75.32	91.24	48.76	56.23
	H_2L_A	74.40	95.32	52.11	66.76
B_1	$Cu(H_2L)I$	57.66	88.3	86.44	92.13
A_1	$Cu(H_2L)I$	88.41	94.31	82.8	86.50
B_2	$Cu(H_2L)_2(ClO_4)_2$	64.5	96.16	70.55	54.92
A_2	$Cu(H_2L)_2(ClO_4)_2$	90.34	94.82	97.63	89.34
B_3	$[Zn\ (H_2L)_2(H_2O)]SO_4$	8.16	96.16	82.16	87.3
A_3	$[Zn\ (H_2L)_2(H_2O)]SO_4$	91.42	93.23	92.6	96.83
B_4	$[Cd\ (H_2L)Cl]Cl$	48.23	58.31	43.66	32.8
A_4	$[Cd\ (H_2L)Cl]Cl$	74.42	65.03	56.63	46.43

The molecular docking

To understand the interaction of all the synthesized molecules with topoisomerase II DNA gyrase enzymes, the crystal structure of topoisomerase II was downloaded from Protein Data Bank (PDB ID: 2XCT) and the molecular docking studies were performed using the Moe program. The protein ligand interaction plays a significant role in structural based drug designing. The different types of interactions are mentioned in Table 9 and seen in Fig. 25. The preferred compounds Cd(II) Cu(II) and Zn(II) complexes had a scoring value of − 5.02, − 9.41 and − 10.87 ,respectively. The Zn(II) complex showed the highest binding affinity and interaction with topoisomerase II DNA gyrase enzymes (2XCT) by using most types of protein binding interactions. The binding affinity of our compounds achieved higher or the same values numerous previous works against the same type of protein [43, 44]. The molecular docking of our work supported that the chelates are more active than their parent ligand against the same microorganism as mentioned also in many of our previous works [45–48].

Table 9
Comparison of binding affinity of complexes against topoisomerase II DNA gyrase enzymes (PDB Code: 2XCT)

Antitumor docking 4jsv		
Compound	**Involved amino acids(scoring energy)**	**Type of interaction**
H_2L_B	Lys-1270(-2.99)	Side chain donor
$[Cu(H_2L)I]$	Asp-1114(-3.30)	Side chain acceptor
$[Cu(H_2L)_2(ClO_4)_2]$	Arg-1299 (-9.41)	Arene-cation interaction
$[Zn(H_2L)_2]SO_4$	Glu-585, Pro-1080, Tyr-1150 and His-1081(-10.87)	Side chain acceptor, Backbone acceptor, Arene-arene and Arene-cation
$[Cd(H_2L)Cl]Cl$	Ser1584(-5.02)	Solvent contact

4. Conclusion

In this work new Cu(I,II), Zn(II) and Cd(II) complexes of thiosemicarbazide ligand (1-(p-(methylanilinocetyl-4-phenyl-thiosemicarbazide) (H_2L_B) have been prepared and characterized by ^{1}HNMR, Mass spectra, IR, elemental analyses, molar conductance, UV-visible spectra, magnetic susceptibility measurements, thermogravimetric analysis (TGA/DTG) and X-ray diffraction pattern before and after γ- irradiation. The biological activity of unirradiated and irradiated compounds were investigated. The results obtained can be summarized as follows:

1**.** The ligand behaves as neutral tridentate , tetradentate or monobasic tetradentate, coordinated to the ligand through the (C=O), N(2)H , (C=S) and coordination take place via enolic oxygen or (C=O) and two N(2)H for complexes(B_2 and B_3).

2. 1H NMR spectra of ligand after irradiation shows higher the intensity of the bands than before irradiation.

3. IR exhibits sharper of the bands and the increase in the stability of the compounds by using radiation

4. X-ray diffraction patterns improve the crystallite size of the complexes by using gamma-irradiation.

5. The proposed structures of complexes were geometrically optimized, also showed that the Cu(I,II), Zn(II) and Cd(II) complexes have four and six coordination geometries; this is also in a good agreement with the experimental results.

6. In vitro antibacterial activity of all synthesized compounds indicated that they are potent antibacterial agents. Besides, This indicate that an increase in the antibacterial activity increases .

7. The molecular docking study supported the antibacterial results.

5. References

1. Tahmeena, K., Rumana, A., Seema, J., & Khan, A. R. (2015). Anticancer potential of metal thiosemicarbazone complexes: a review. *Der Chemica Sinica*, *6*, 1-11.
2. Tada, R., Chavda, N., & Shah, M. K. (2011). Synthesis and characterization of some new thiosemicarbazide derivatives and their transition metal complexes. *Journal of Chemical and Pharmaceutical Research*, *3*(2), 290-297.
3. Scovill, J. P., Klayman, D. L., & Franchino, C. F. (1982). 2-Acetylpyridine thiosemicarbazones. 4. Complexes with transition metals as antimalarial and antileukemic agents. *Journal of Medicinal Chemistry*, *25*(10), 1261-1264.
4. Krishna, P. M., & Reddy, K. H. (2009). Synthesis, single crystal structure and DNA cleavage studies on first 4 N-ethyl substituted three coordinate copper (I) complex of thiosemicarbazone. *Inorganica Chimica Acta*, *362*(11), 4185-4190.
5. Abou Sekkina, M. M. A., Kashar, T. I., & Aly, S. A. (2011). Spectrochemical study and effect of high energatic gamma ray on copper(II) complexes. Solid State Sciences, 13(12), 2080-2085.
6. Abou Sekkina, M.M. El-Boraey, H. A., & Aly, S. A. (2014). Further studies on the properties and effect of high energetic ionizing radiation on copper(II) complexes: ^{1}H NMR, electronic absorption, ESR spectra and solid electrical conductivity. Journal of Radioanalytical and Nuclear Chemistry, 300(2), 867-872.
7. Aly, S. A., and Elembaby, D. (2020) : Synthesis, spectroscopic characterization and Study the effect of gamma irradiation on VO^{2+}, Mn^{2+}, Zn^{2+}, Ru^{3+}, Pd^{2+}, Ag^{+} and Hg^{2+} complexes and antibacterial activities. Arbian, J. 13, 4425-4447.
8. Hanaa.A. El-Boraey, M.A. Abdel-Hakeem, Facile synthesis, spectral, EPR, XRD and antimicrobial screening of some γ- irradiated N', N'''-(1E, 2E)-1,2-diphenylethane-1,2-diylidene)bis(2aminobenzohydrazide) metal complexes. *J. Mol. Struct.* 1211 (2020) 128086.
9. Hanaa. A. El-Boraey, O. A. El-Gammal, N. G. Abdel Sattar, Impact of gamma ray irradiation on some aryl amide bridged Schiff base complexes: spectral, TGA, XRD and antioxidant property, *J. Radioanal. Nucl. Chem.* 323 (2020) 241–252.
10. Heba. Alshater, H. A. El-Boraey, A. M.A. Homoda, O. A. EL-Gammal, Improving the surface morphology and crystallite size of isonicotinohydrazide based binuclear Cr(III), Zn(II) and Sn(IV) complexes after irradiation with *γ* –rays. *J. Mol. Struct.* 1232 (2021) 129985.
11. West, D, (1996). Complexometry with EDTA and related reagents (46, 164). BDH Chemicals Limited
12. Wallingford, CT GaussView 5.0, (Gaussian Inc. 2009
13. Wallingford, CT Gaussian 09 rev. A.02, (Gaussian Inc. 2009
14. Aly,S.A., El-Boraey, A.H, (2019). Effect of gamma irradiation on spectral, XRD, SEM, DNA binding, molecular modling and antibacterial property of some (Z)eN-(furan-2-yl)methylene)-2-(phenylamino)acetohydrazide metal(II) complexes. Journal of Molecular Structure 1185 :323-332.
15. Elhalafawy K, Guirgis A, Elkousy S, Rizk N,and Eldourghamy A (2009). Purification and characterization of streptokinase produced by s. pyogens and s. equisimilis .Sci. J. Fac. Sci. Minufia Univ(23), 85-103.
16. El-Boraey H , El-Salamony M, Hathout A,(2016). Macrocyclic [N5] transition metal complexes:synthesis, characterization and biological activities J InclPhenom Macrocycl Chem 86:153–166.
17. Bayoumi , H.A., Alaghaz ,A.M .A., & Aljahdali , M .S.(2013). Cu(II), Ni(II), Co(II) and Cr(III) complexes with N_2o_2 -chelating Schiff's base ligand incorporating azo and sulfonamide moieties: spectroscopic, electrochemical

behavior and thermal decomposition studies. Int. J. Electrochem Sci, (8), 9399–9413 .

18. Kong D, Xie Y. (2002).Synthesis, structural characterization of tetraazamacrocyclic ligand, five-coordinated zinc(II) complexes. Inorg Chim Acta. , 338, 142–148.
19. Geary, W.G. (1971).The use of conductivity measurements in organic solvents for the characterization of coordination compounds. Coord Chem Rev.,7,81–122.
20. Aly, S.A. (2017). Spectrochemical Study the Effect of High Energetic Ionization Radiation on Ru(III), Pd(II) and Hg(II) Complexes.. Journal of Radiation Research and Applied Science, 10, 89-96.
21. AbouSekkina, M. M. A., Kashar, T. I., & Aly, S. A. (2011). Spectrochemical study and effect of high energatic gamma ray on copper(II) complexes. Solid State Sciences, 13(12), 2080-2085.
22. Nakamoto, K. (1970). Infrared spectra of inorganic and coordination compounds.New alicyclic thiosemicarbazone chelated zinc (II) antitumor complexes: Interactions with DNA/protein, nuclease activity and inhibition of topoisomerase-I. Polyhedron, 105, 89-95.
23. El-Boraey, H. A., El-Salamony, M. A., & Hathout, A. A. (2016). Macrocyclic [N_5] transition metal complexes: synthesis, characterization and biological activities. Journal of Inclusion Phenomena and Macrocyclic Chemistry, 86(1-2), 153-166.
24. Aly, S.A. (2017). Spectrochemical Study the Effect of High Energetic Ionization Radiation on Ru(III), Pd(II) and Hg(II) Complexes.. Journal of Radiation Research and Applied Science, 10, 89-96.
25. Seena, E. B., & Kurup, M. P. (2008). Synthesis, spectral and structural studies of zinc(II) complexes of salicylaldehyde N (4)-phenylthiosemicarbazone. Spectrochimica Acta Part A: Molecular and Biomolecular Spectroscopy, 69(3), 726-732.
26. Rafı, U. M., Mahendiran, D., Kumar, R. S., & Rahiman, K. (2019). Metal complexes of tetradentate azo-dye ligand derived from 4,4'-oxydianiline: Preparation, structural investigation, biological evaluation and MOE studies .Appl.Organomet. Chem. 33(7), e4946-4966.
27. Pathaw, L., Maheshwaran, D., Nagendraraj, T., Khamrang, T., Velusamy, M., & Mayilmurugan, R. (2021). Tetrahedral copper(I) complexes of novel N,N-bidentate ligands and photophysical properties Inorganica Chimica Acta,514, 119999.
28. Ahmed, M., Khalid, W.Y., & Zain, A.(2012) Synthesis and Characterization of new thio-Triazole ligand and complexes with selected metals. J. Pharma. Biol. Sci., 4, 09.
29. Sharma, M., Ganeshpandian, M., Majumder, M., Tamilarasan, A., Sharma, M., Mukhopadhyay,R., Islam, Nashreen S. & Palaniandavar, M . (2020). Octahedral copper(II)-diimine complexes of triethylenetetramine: effect of stereochemical fluxionality and ligand hydrophobicity on CuII/CuI redox, DNA binding and cleavage, cytotoxicity and apoptosis-inducing ability. Dalton Trans., 49, 8282-8297.
30. Leblanc ,M., Gonzalez-Sarrıas ,A., ´ Beckford, F. A., Mbarushimana ,P. C. & Seeram, P. N. (2011). Coordination Chemistry of Polyaromatic Thiosemicarbazones 2: Synthesis and Biological Activity of Zinc, Cobalt, and Copper Complexes of 1-(Naphthalene-2-yl)ethanone Thiosemicarbazone. International Journal of Inorganic Chemistry ,2011, Article ID 624756, 1-8 .
31. Paira, M. K., Dinda, J., Lu, T. H., Paital, A. R. & Sinha, C. (2007). Zn (II), Cd (II) and Hg (II) complexes of 8-aminoquinoline.: Structure, spectra and photoluminescence property. Polyhedron, 26(15), 4131-4140.
32. Azam, M., Al-Resayes, S. I., & Pallepogu, R. (2016). Synthesis and Structural Characterization of Cadmium (II) and Mercury (II) Complexes Derived from 3-Aminoquinoline. *Helvetica Chimica Acta*, *99*(1), 20-23.

33. Sen, S., Saha, M. K., Kundu, P., Mitra, S., Kruger, C., &Bruckmann, J. (1999). Synthesis and structure of a heptacoordinated cadmium (II) complex. Inorganica chimica acta, 288(1), 118-121.
34. Huang,B. L., Perez, R. J., Lavernia, E. J., & Luton, M. J. (1996). Formation of supersaturated solid solutions by mechanical alloying. Nanostructured Materials, 7(1), 67-79.
35. Al-Ashqer, S., Abou-Melha, K. S., Al-Hazmi, G. A. A., Saad, F. A., & El-Metwaly, N. M. (2014). Spectral studies on a series of metal ion complexes derived from pyrimidine nucleus, TEM, biological and γ-irradiation effect. Spectrochimica Acta Part A: Molecular and Biomolecular Spectroscopy, 132, 751-761.
36. Jayashri, T. A., Krishnan, G., & Rema Rani, N. (2014). Effect of gamma-irradiation on thermal decomposition kinetics, X-ray diffraction pattern and spectral properties of tris (1, 2-diaminoethane) nickel(II) sulphate. Radiation Effects and Defects in Solids, 169(12), 1019-1030.
37. Jeslin Kanaga Inba, P., Annaraj, B., Thalamuthu, S. &Neelakantan, M. A. (2013). Cu (II), Ni (II), and Zn (II) complexes of salan-type ligand containing ester groups: synthesis, characterization, electrochemical properties, and in vitro biological activities. *Bioinorganic Chemistry and Applications*, *2013*.
38. Sharma, A. & Shah, M. (2013). Synthesis and characterization of some transition metal complexes derived from bidentate Schiff base ligand. Journal of Applied Chemistry, 3, 62-66.
39. Tweedy, B. G. (1964). Plant extracts with metal ions as potential antimicrobial agents. Phytopathology, 55, 910-914.
40. Sönmez, M., Celebi, M., & Berber, I. (2010). Synthesis, spectroscopic and biological studies on the new symmetric Schiff base derived from 2, 6-diformyl-4-methylphenol with N-aminopyrimidine. European Journal of Medicinal Chemistry, 45(5), 1935-1940.
41. Chohan, Z. H., Shaikh, A. U., Rauf, A., & Supuran, C. T. (2006). Antibacterial, antifungal and cytotoxic properties of novel N-substituted sulfonamides from 4-hydroxycoumarin. Journal of Enzyme Inhibition and Medicinal Chemistry, 21(6), 741-748.
42. Singh, N. K. (2014). Manganese(II) and zinc(II) complexes of 4-phenyl (2-methoxybenzoyl)-3-thiosemicarbazide: Synthesis, spectral, structural characterization, thermal behavior and DFT study. Polyhedron, 73, 98-109.
43. Pisano,M. B., Kum, A., Medda, R., Gianluca Gatto,G., Pal,R., Fais, A., Benedetta Era, B., Cosentino, S., Uriarte, E., Santana,L., Pintus, F., and Matos, M. J. Antibacterial Activity and Molecular Docking Studies of a Selected Series of Hydroxy-3-arylcoumarins Molecules 2019, 24, 2815
44. El-Etrawy, A.,Sherbiny, F. F., Design, synthesis, biological assessment and molecular docking studies of some new 2-Thioxo-2,3-dihydropyrimidin-4(1*H*)-ones as potential anticancer and antibacterial agents, Journal of Molecular Structure, 1225, 5 , 2021, 129014.
45. Hassan, S. S., Antibacterial, DFT and molecular docking studies of Rh(III) complexes of Coumarinyl-Thiosemicarbazone nuclei based ligands Appl. Organomet. Chem. 2017, 32, 1.
46. Hassan, S. S. and Gomha, S. M., Novel functionalized thiosemicarbazone ligands and their Pd(II) complexes: synthesis, characterization, antibacterial and cytotoxic activities Chem. Pap. 2018, 73, 331.
47. Hassan, S. S. and Mohamed, E. F. Antimicrobial, antioxidant and antitumor activities of Nano Structure Eu(III) and La(III) complexes with nitrogen donor tridentate ligands Appl Organometal Chem. 2020
48. Khalf-Alla, P. A., Basta, A. H., Lotfy, V. F. and Hassan, S. S. Synthesis, Characterization, Speciation, and Biological Studies on Metal Chelates of Carbohydrates with Molecular Docking Investigation, Macromol.

Mater. Eng. 2021, 306.

Figures

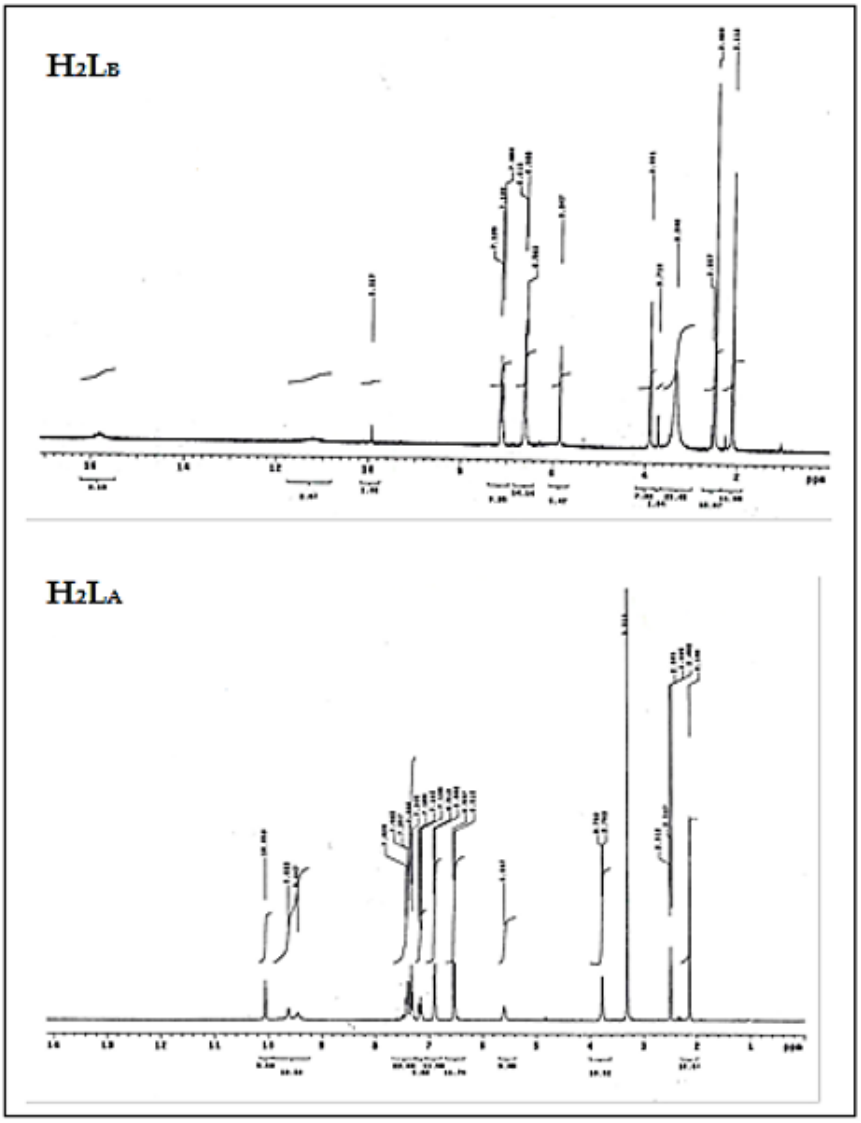

Figure 1

1H NMR spectra of ligands (H2LB) before and after irradiation (H2LA) in DMSO-d6 solution

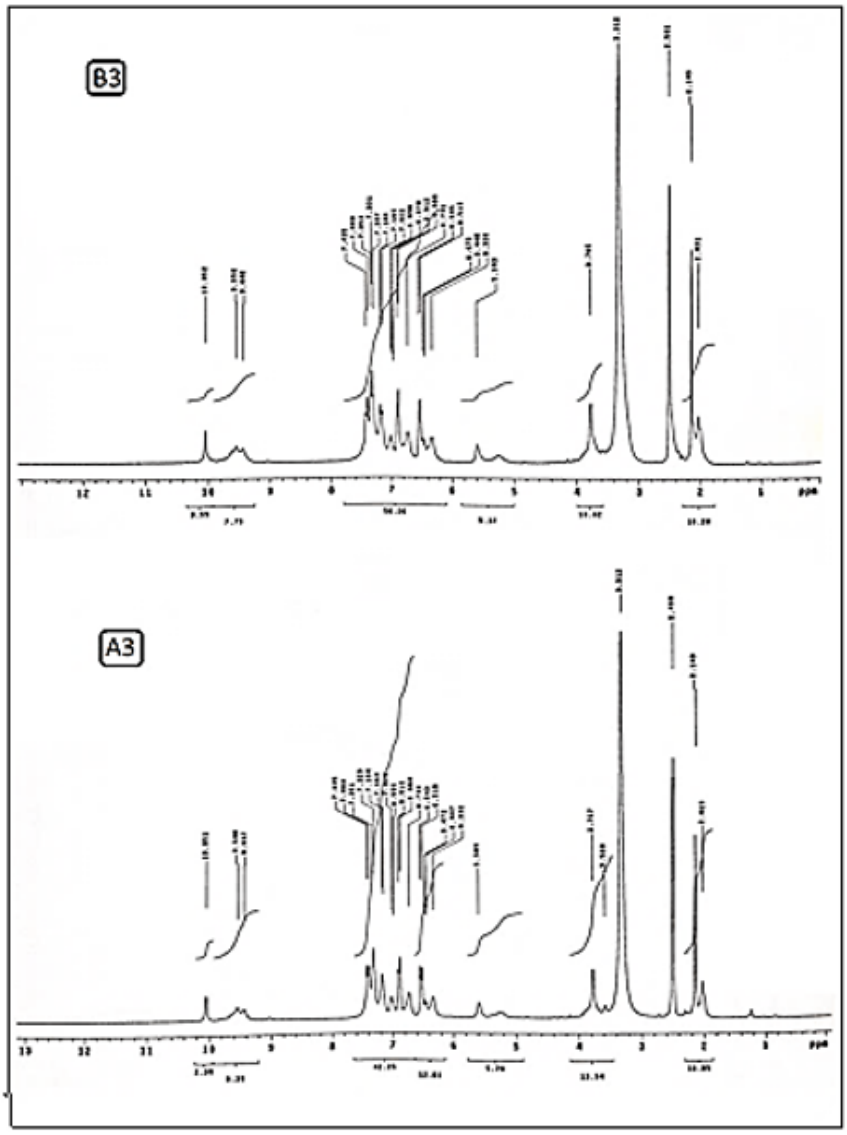

Figure 2

1H NMR spectra of complexes B3 before and after irradiation A3 in DMSO-d6 solution

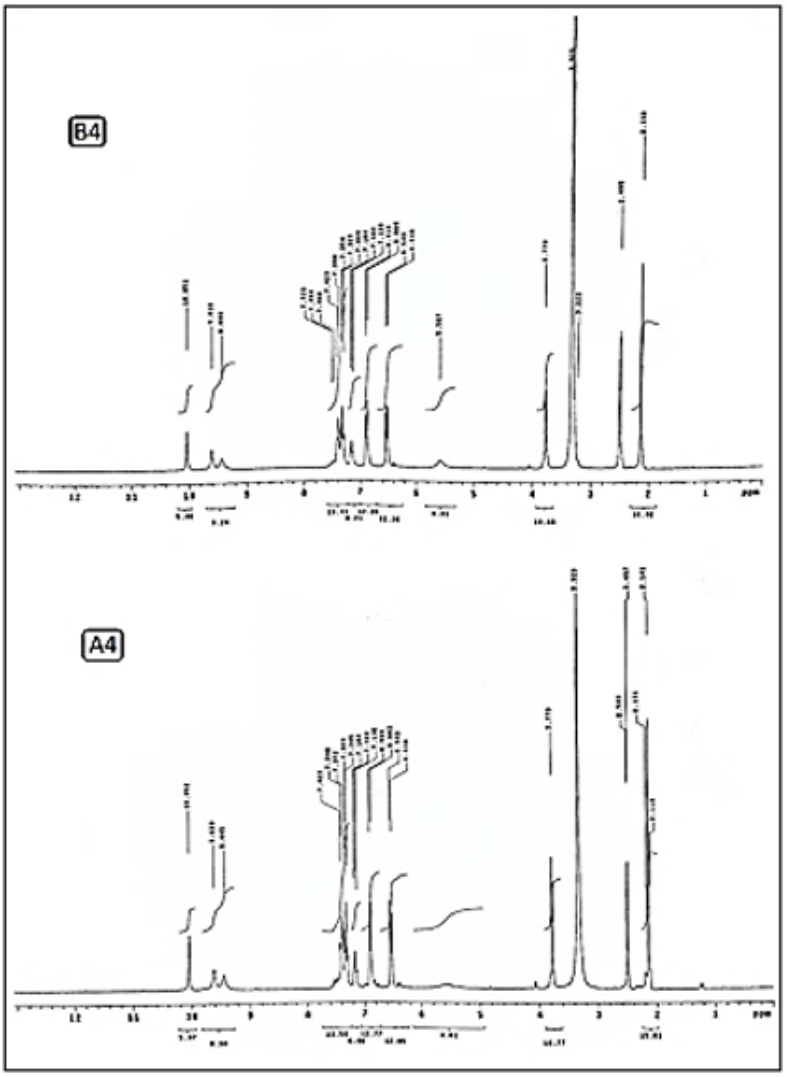

Figure 3

1H NMR spectra of cadium complex (B4) before and after irradiation (A4) in DMSO-d6 solution

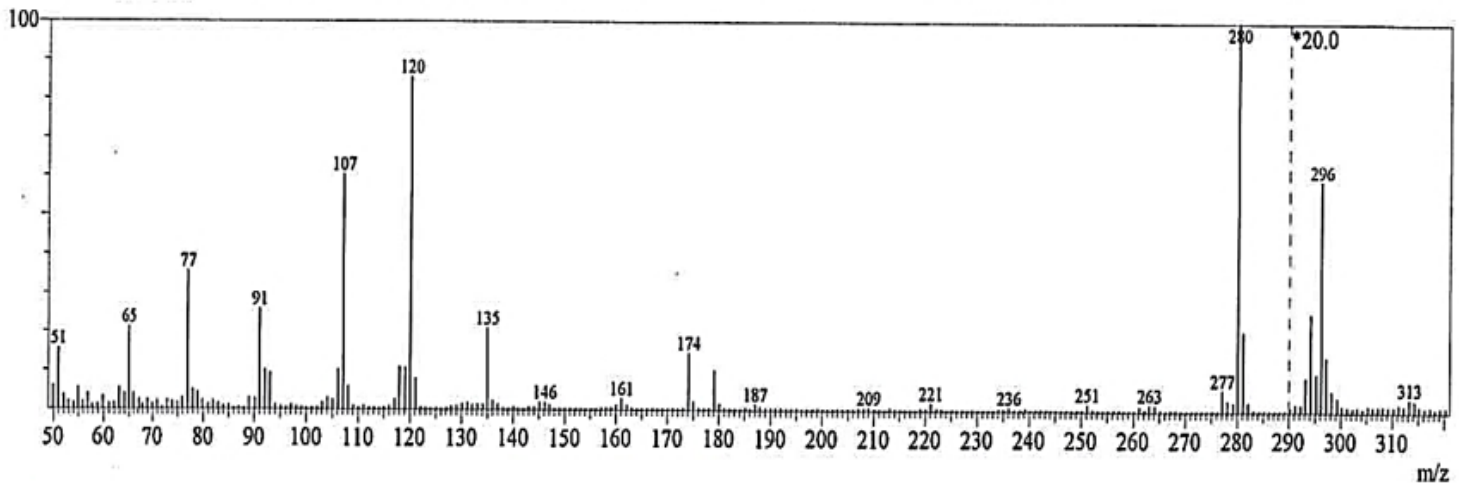

Figure 4

Mass spectrum of ligand (H2LB)

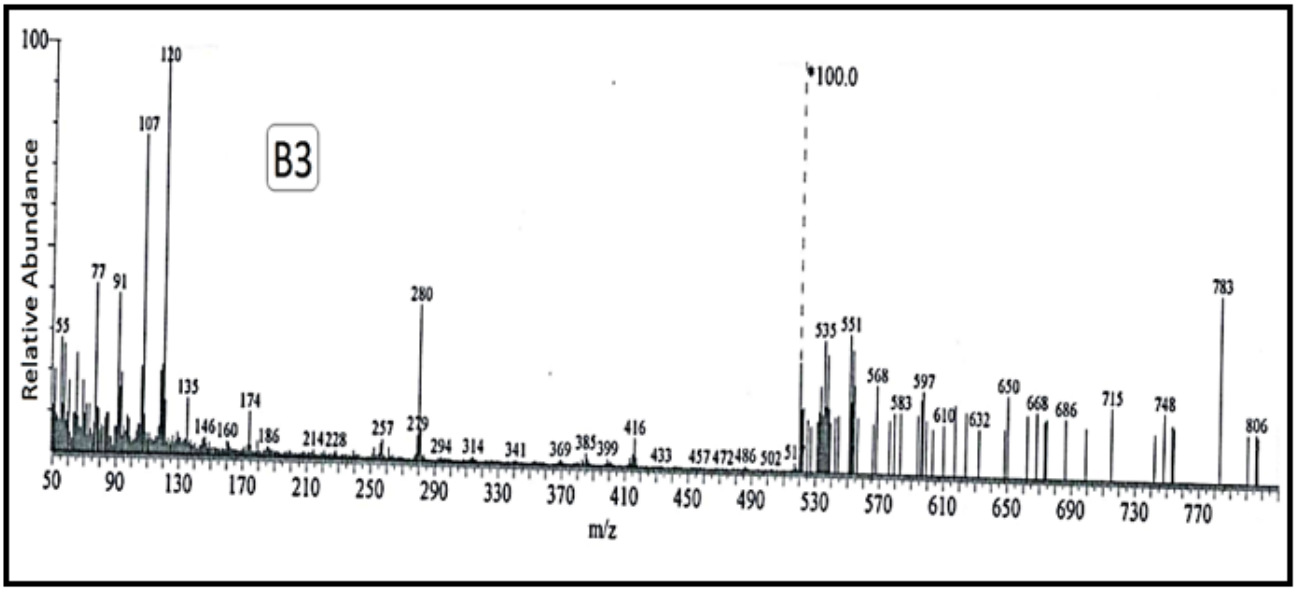

Figure 5

Mass spectrum of zinc complex (B3)

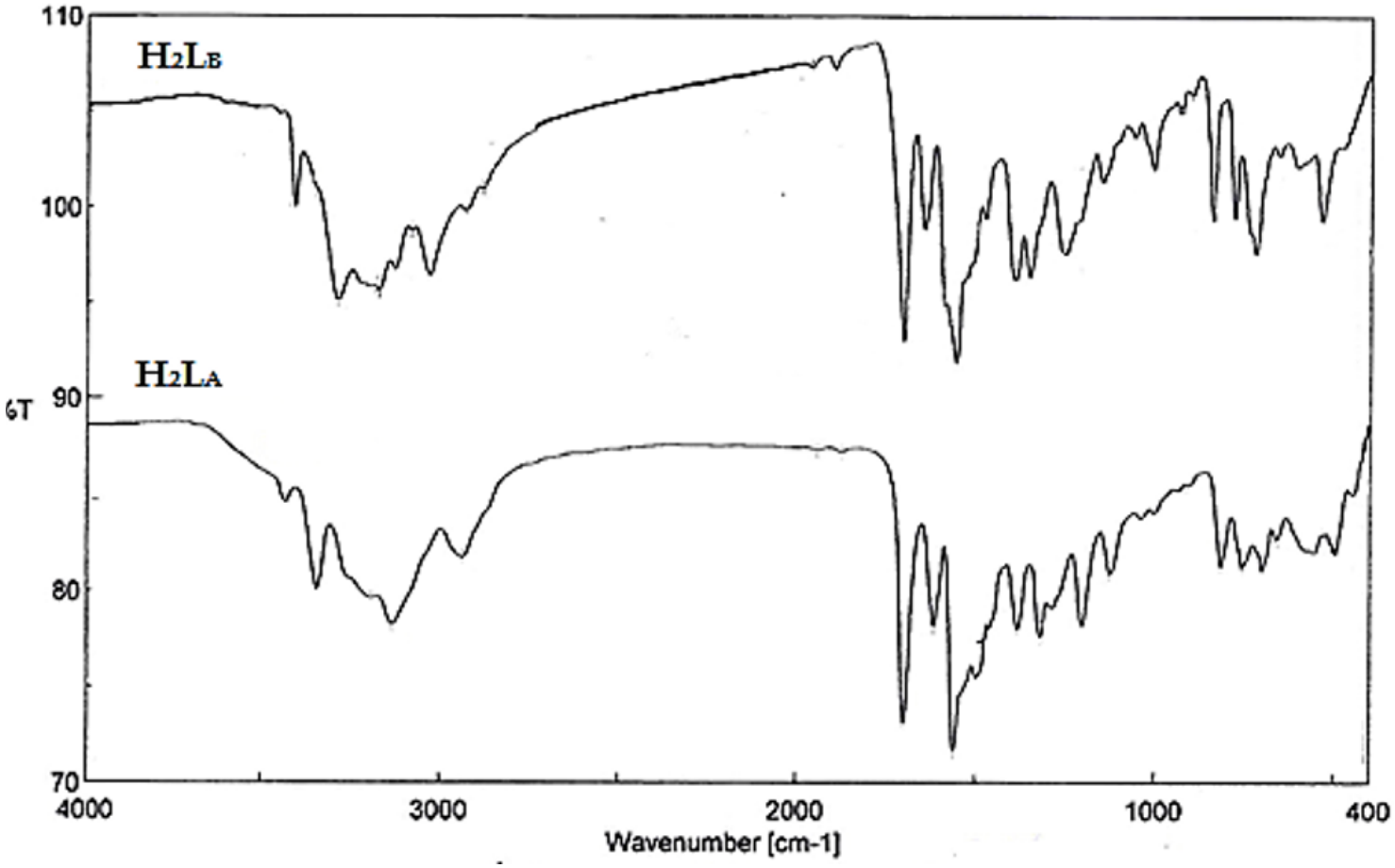

Figure 6

IR spectra of the ligand (H2LB) before irradiation and after irradiation (H2LA)

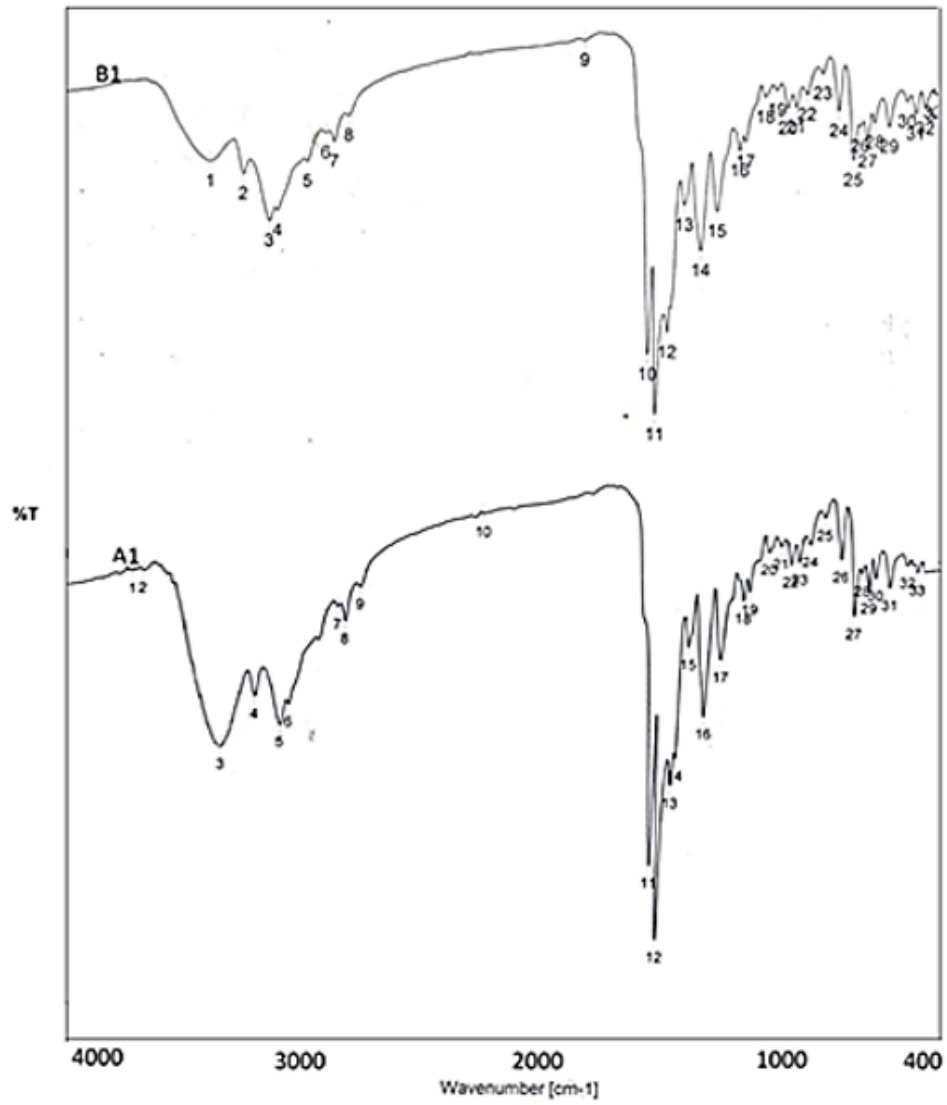

Figure 7

IR spectra of copper(I) complexes before irradiation (B1) and after irradiation (A1)

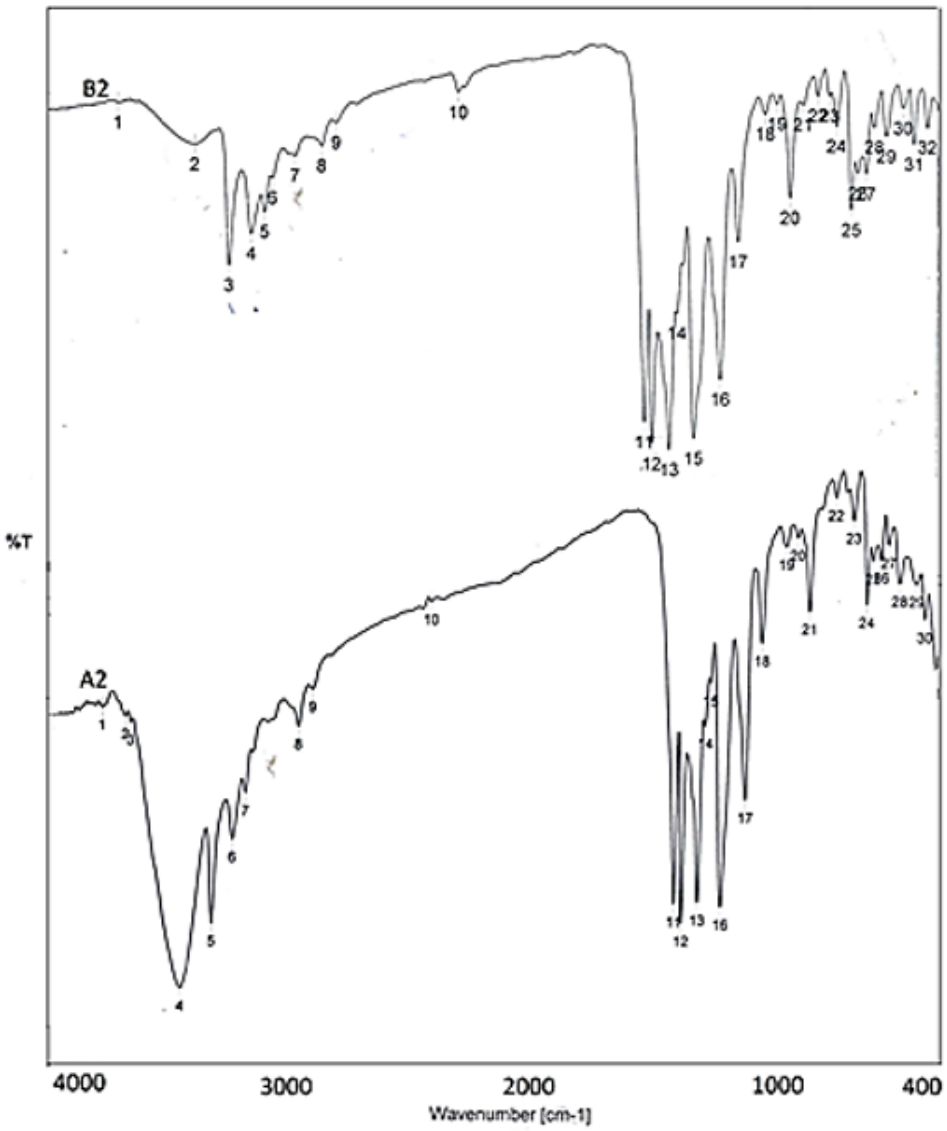

Figure 8

IR spectra of copper(II) complexes before irradiation (B2) and after irradiation (A2)

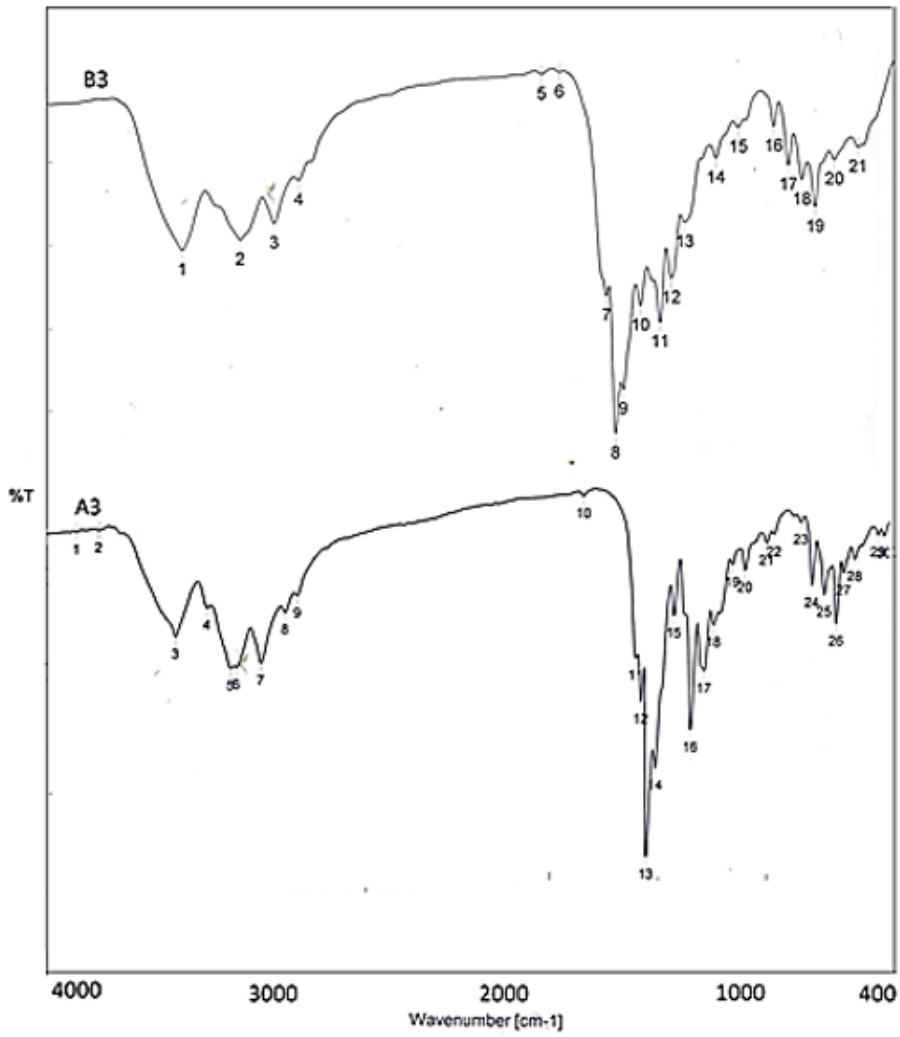

Figure 9

IR spectra of zinc complexes before irradiation (B3) and after irradiation (A3)

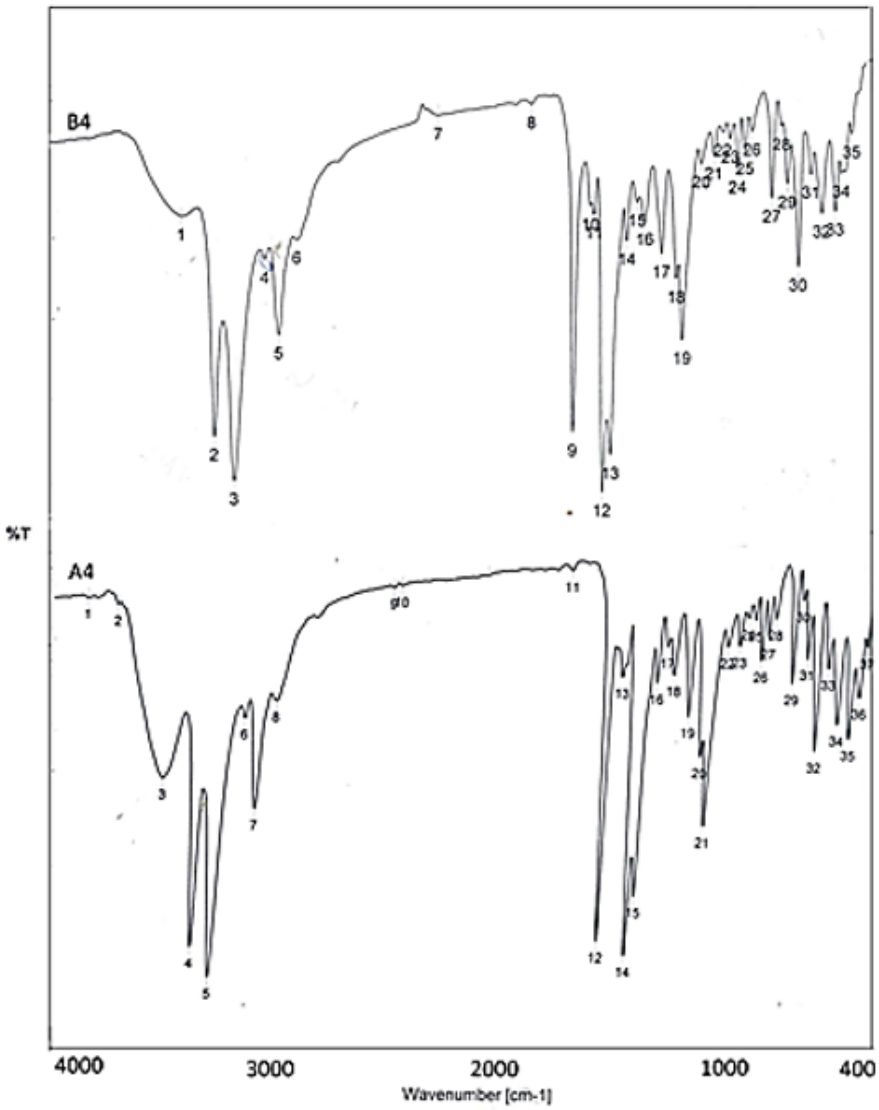

Figure 10

IR spectra of Cadium complexes before irradiation (B4) and after irradiation (A4)

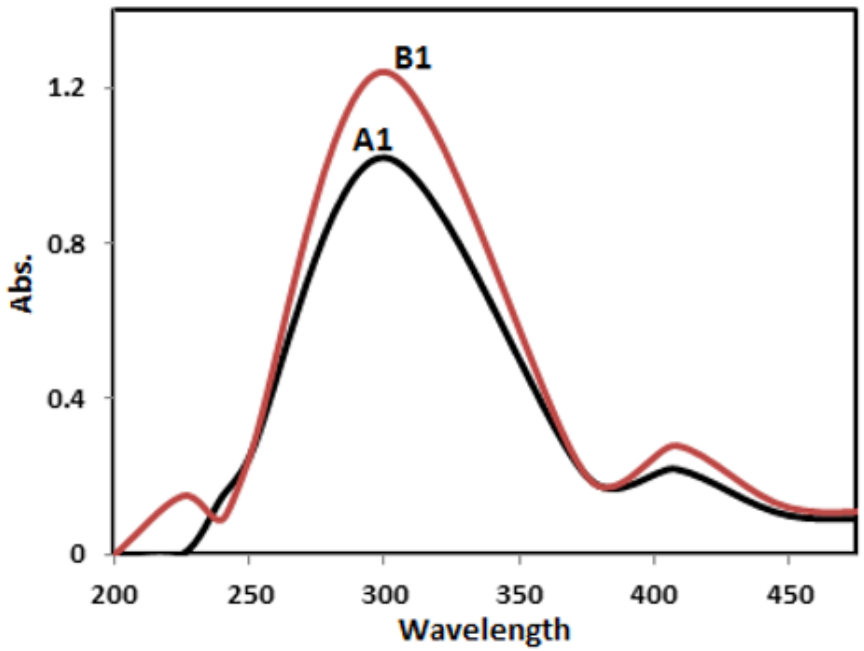

Figure 11

UV- spectra of copper complexes before and after irradiation(B1 and A1)

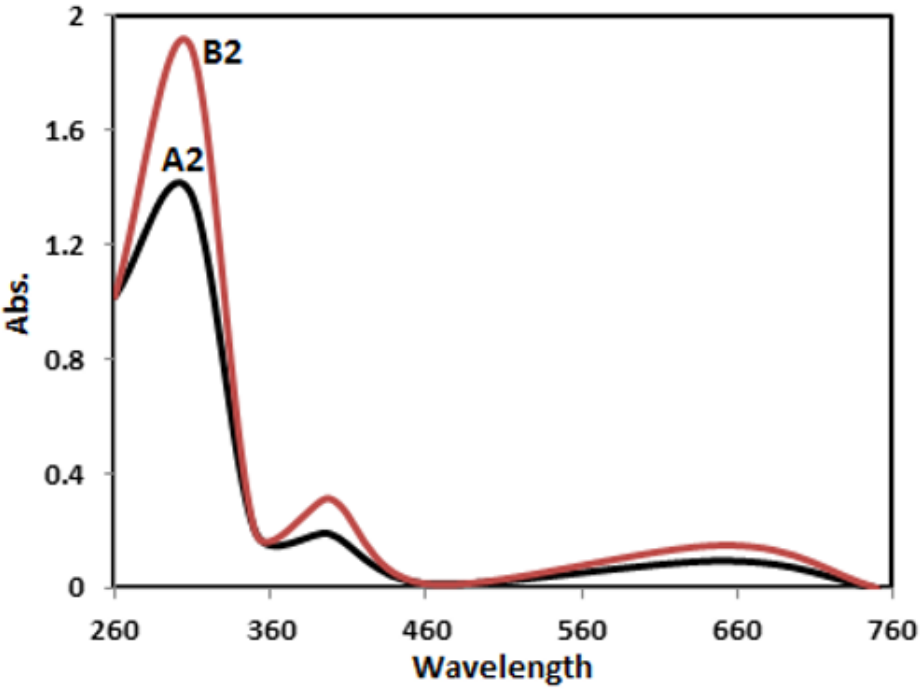

Figure 12

UV- spectra of copper complexes before and after irradiation(B2and A2)

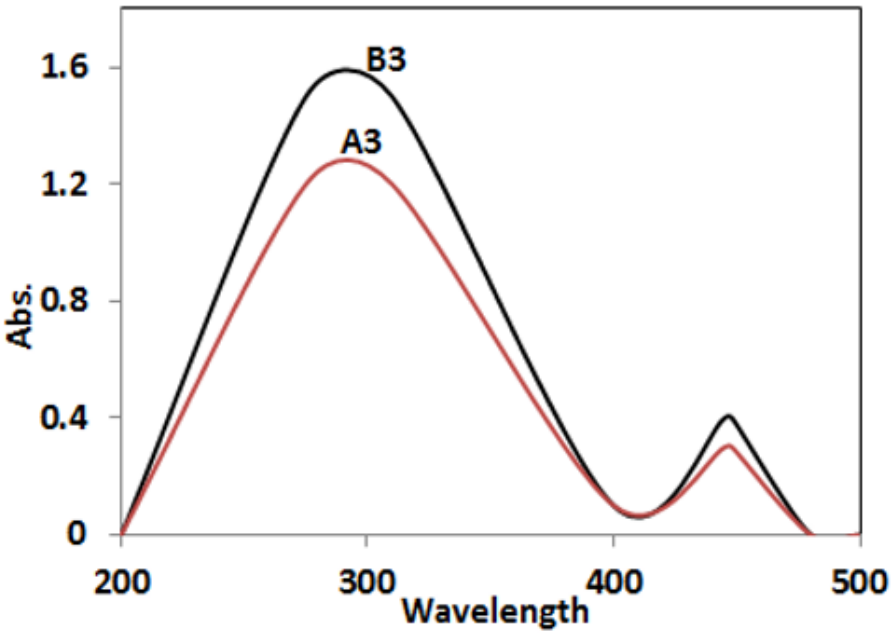

Figure 13

UV- spectra of zinc(II) complexes before and after irradiation(B3and A3)

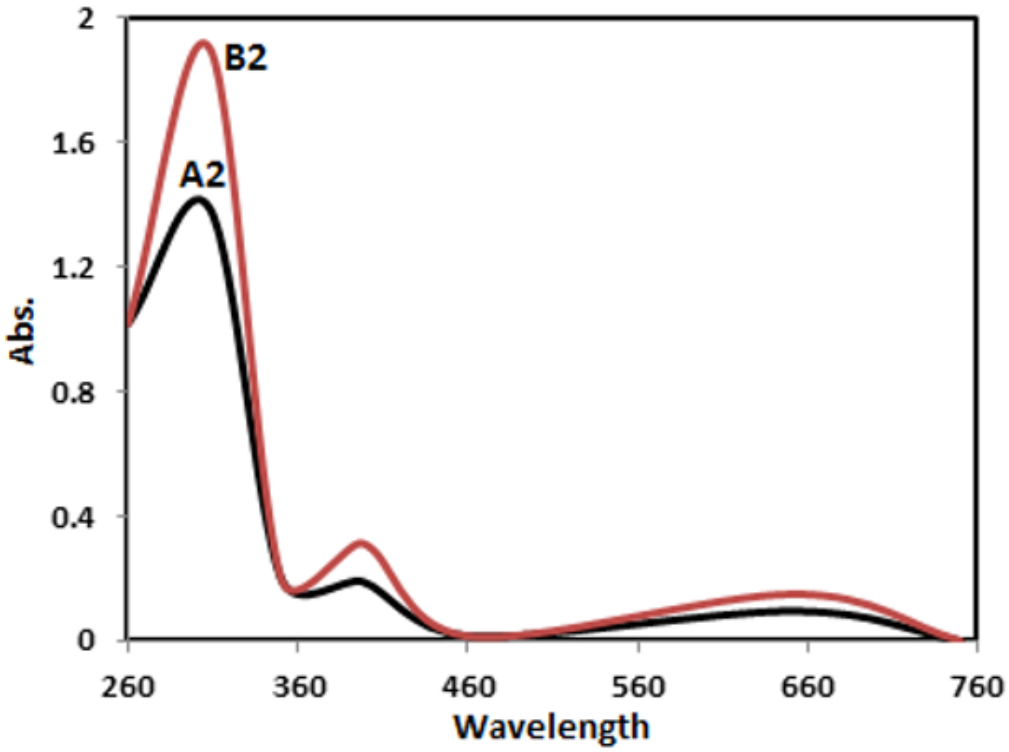

Figure 14

UV- spectra of Cd(II) complexes before and after irradiation(B4 and A4)

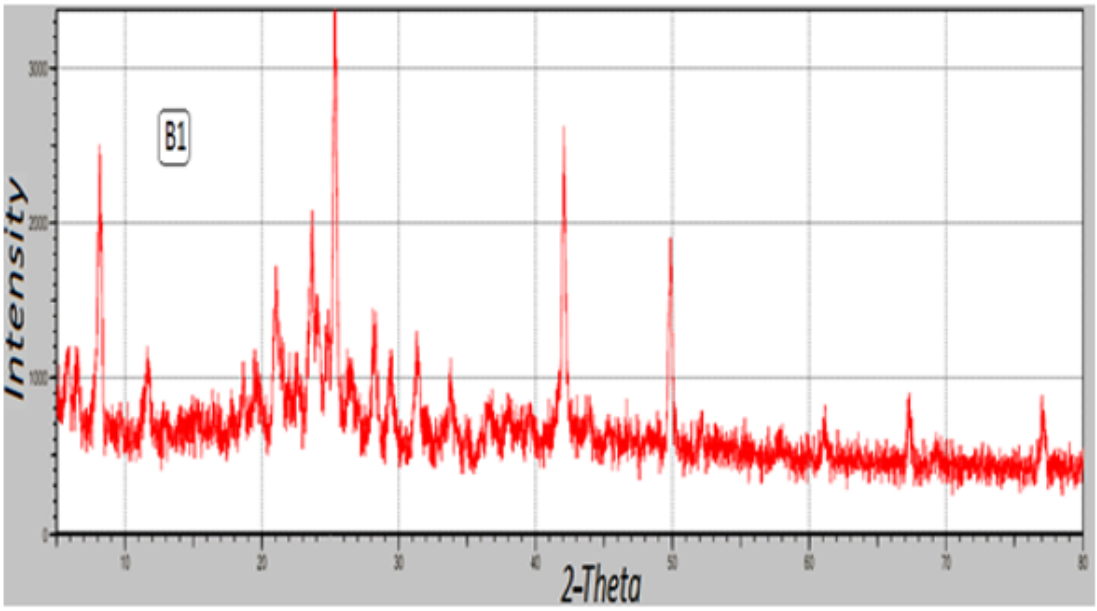

Figure 15

XRD spectra of copper(I) complex before irradiation(B1)

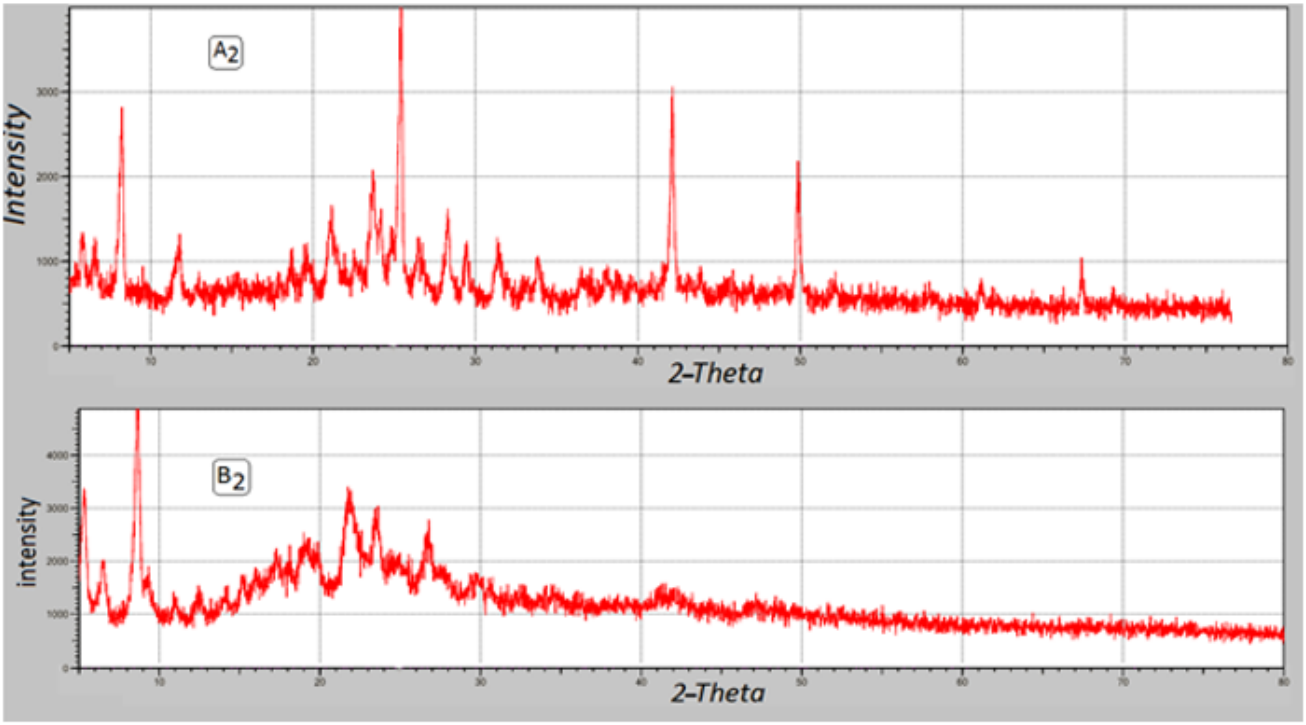

Figure 16

XRD spectra of copper(II) complexes before and after irradiation(B2 and A2)

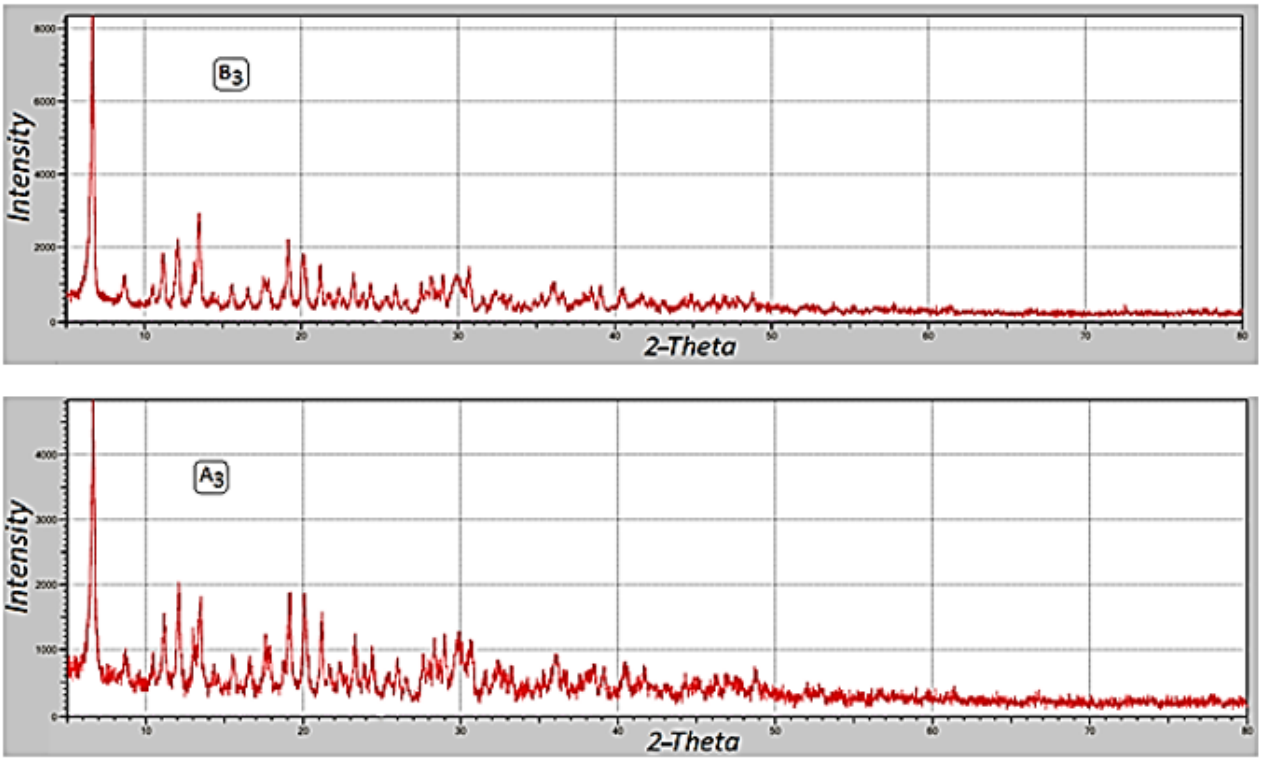

Figure 17

XRD spectra of zinc(II) complexes before and after irradiation(B3 and A3)

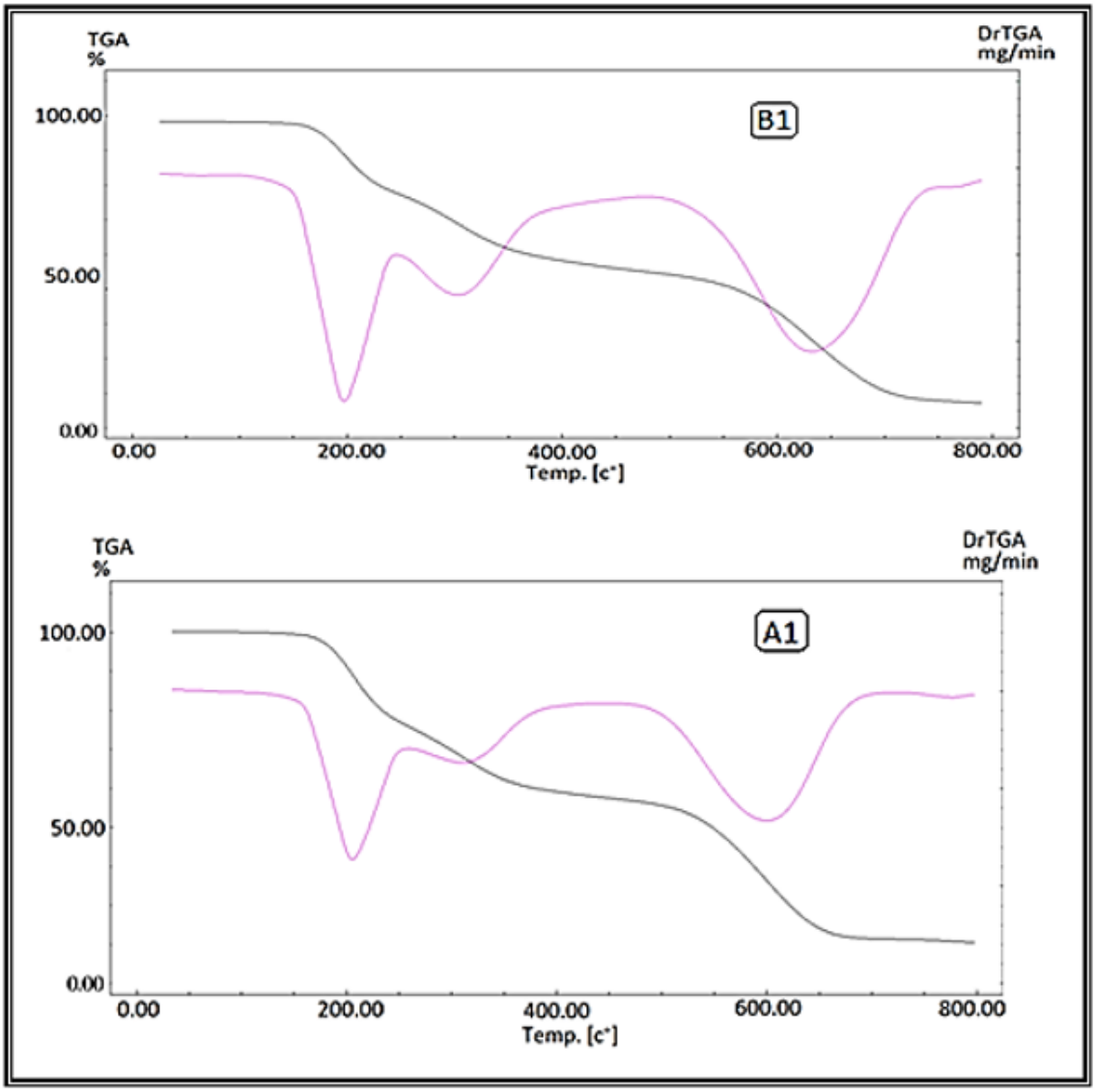

Figure 18

TGA/ DTG curves of complexes before irradiation (B1), after irradiation (A1)

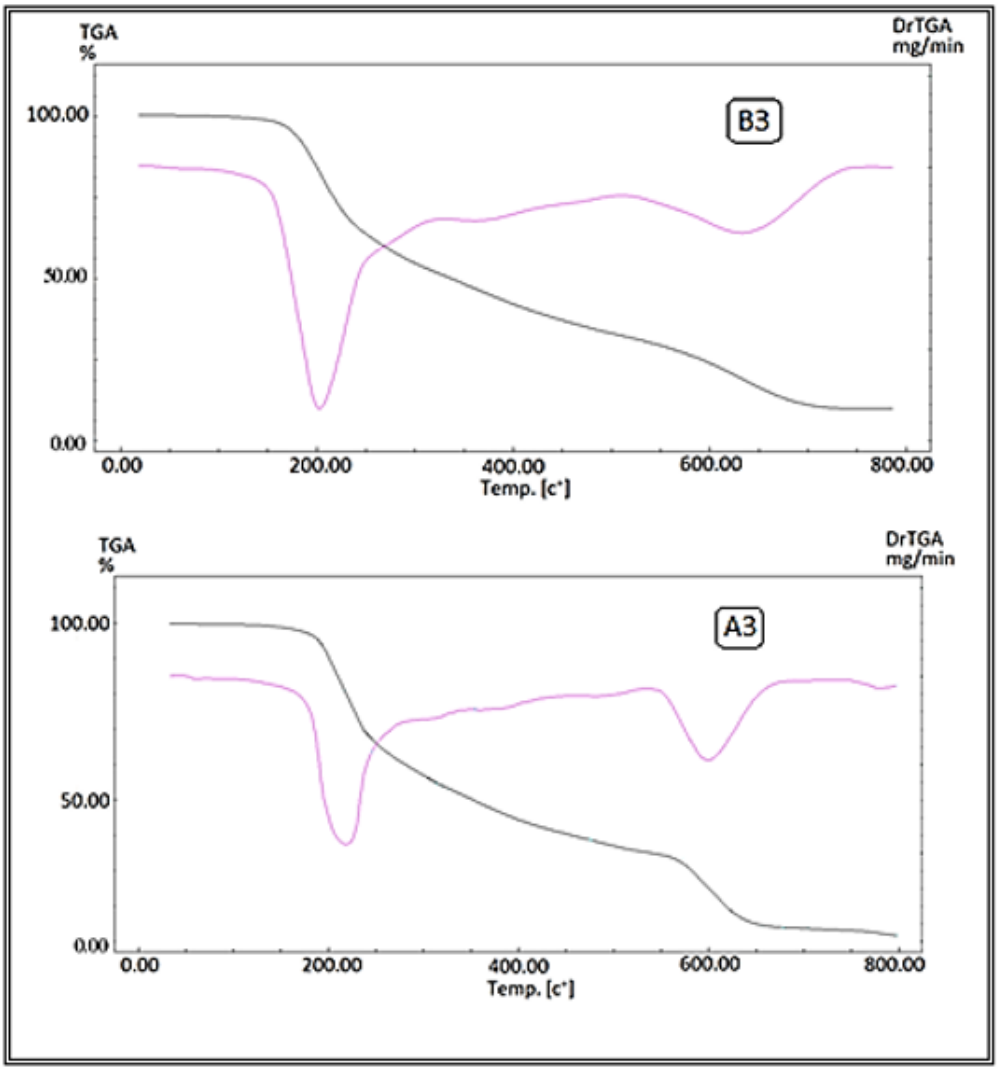

Figure 19

TG/ DTG curves of complexes (B3) before irradiation, after irradiation (A3)

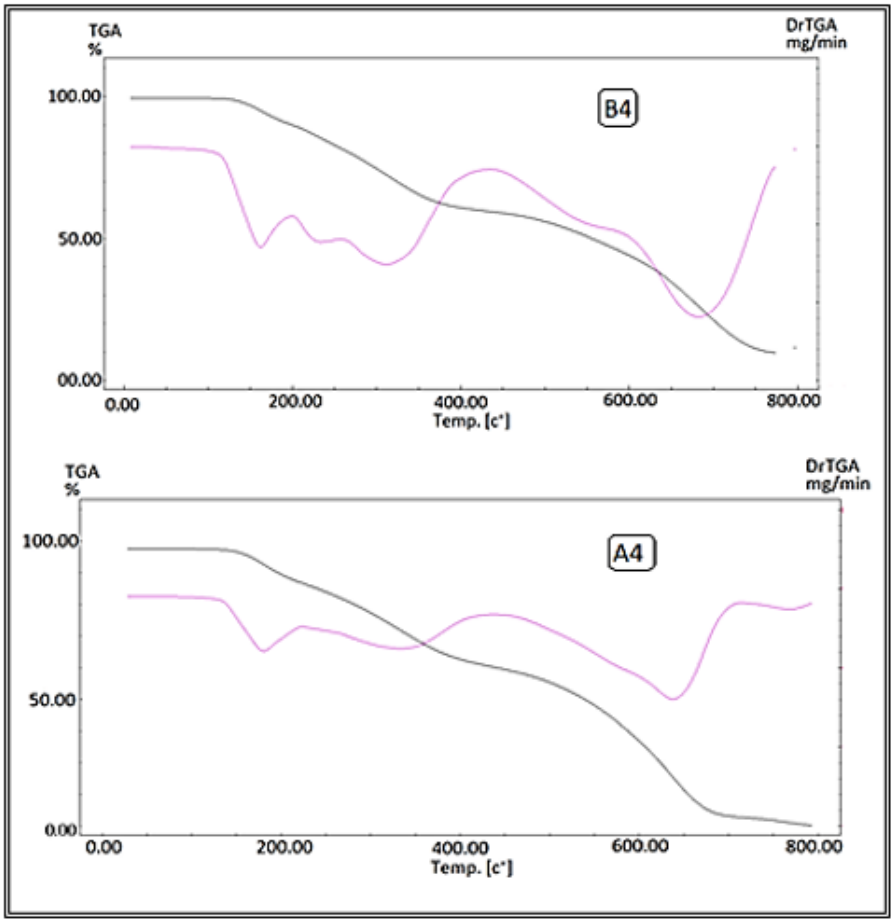

Figure 20

TG/ DTG curves of complexes (B4) before irradiation, after irradiation (A4)

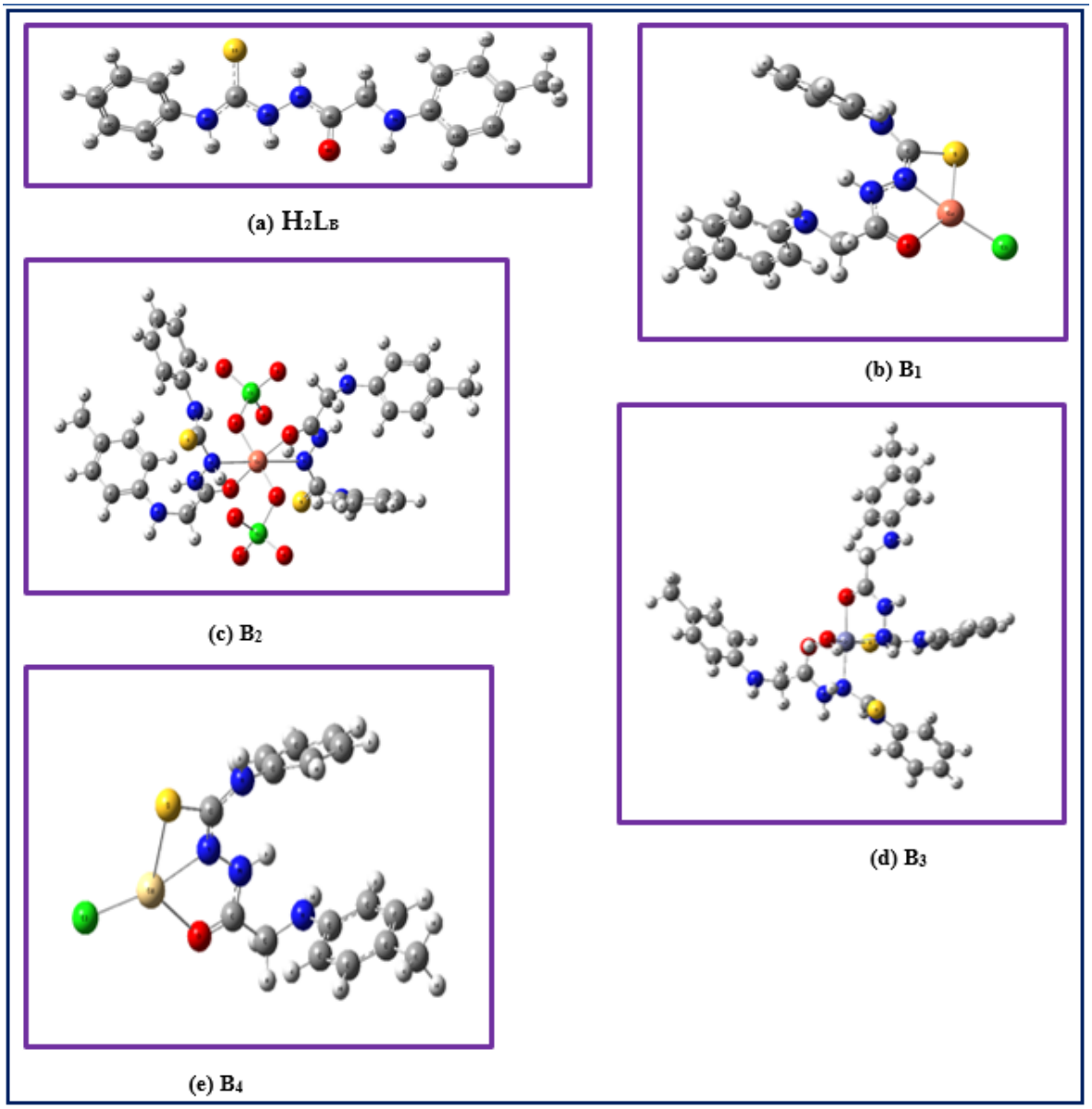

Figure 21

Optimized 3D structures of ligand (a) H2LB, (b))[Cu(H2L)I], (c) [Cu(H2L)2ClO4], (d) [Zn (H2L)2(H2O)]SO4 and (e) [Cd(H2L)Cl]Cl.

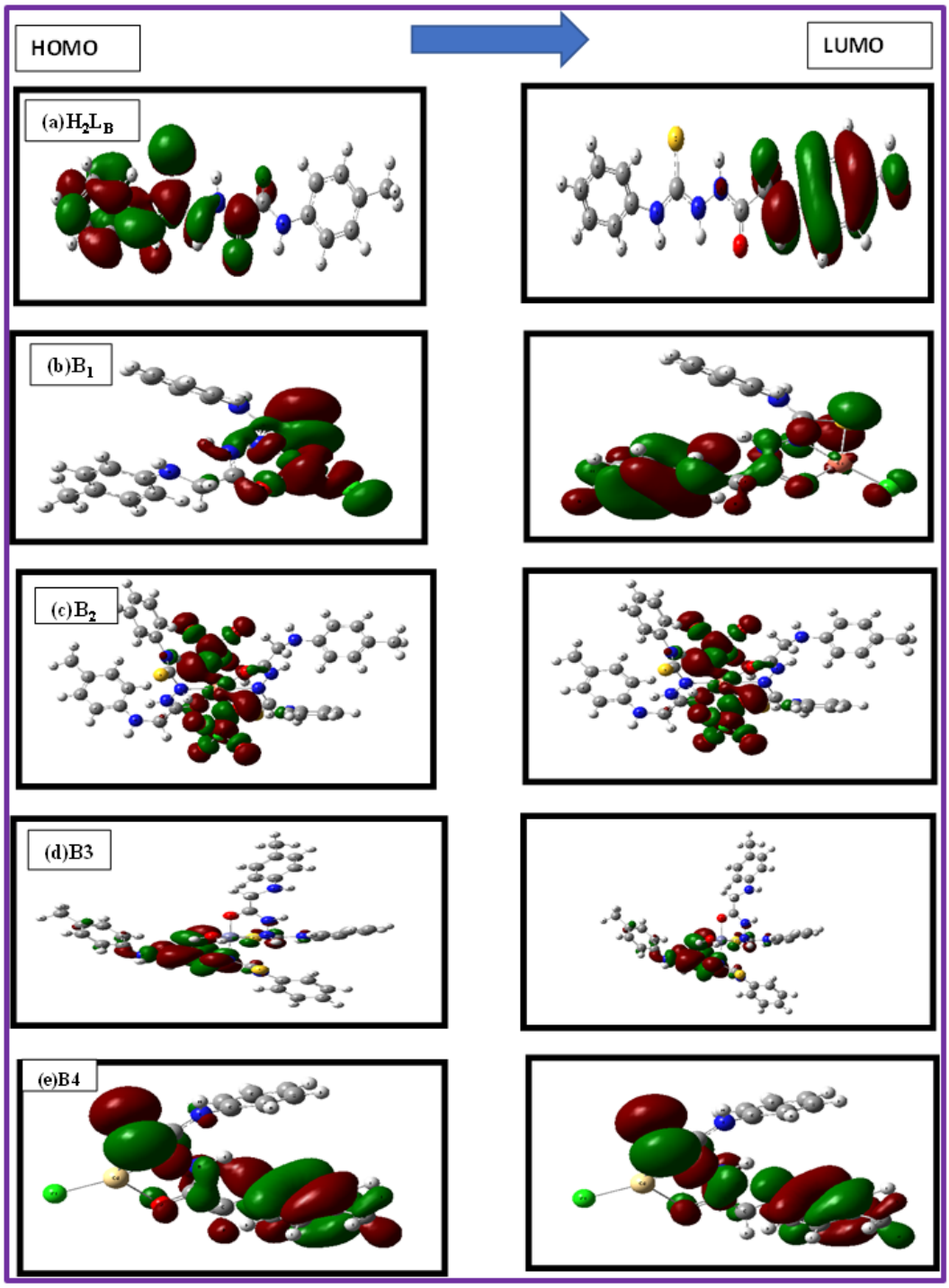

Figure 22

Frontier HOMO and LUMO molecular orbitals for ligand (a) H2LB, (b) B1= [Cu(H2L)I], (c) B2= [Cu(H2L)2ClO4], (d) B3 = [Zn(H2L)2ClO4] and (e) B4 = [Cd(H2L)Cl]Cl complexes calculated at DFT level.

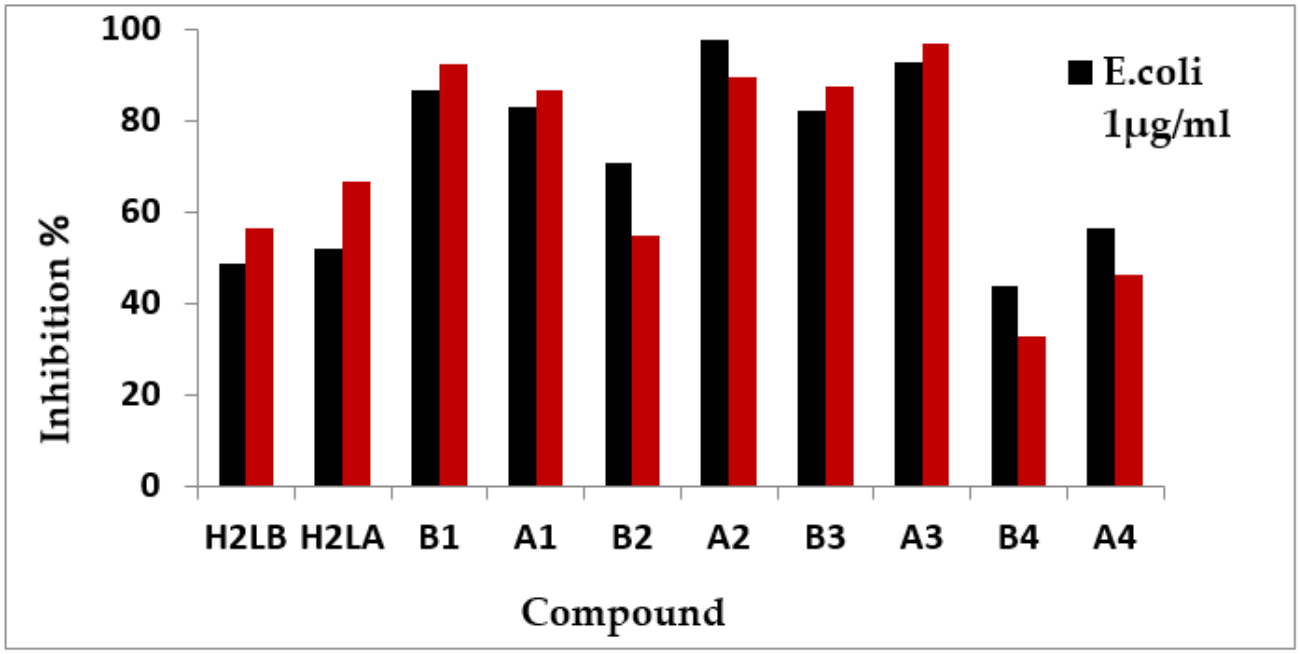

Figure 23

Antibacterial activity for ligand and copper, zinc and cadium (B1, B2,B3,B4 and A1,A2,A3, A4) complexes before and after irradiation against E. coli

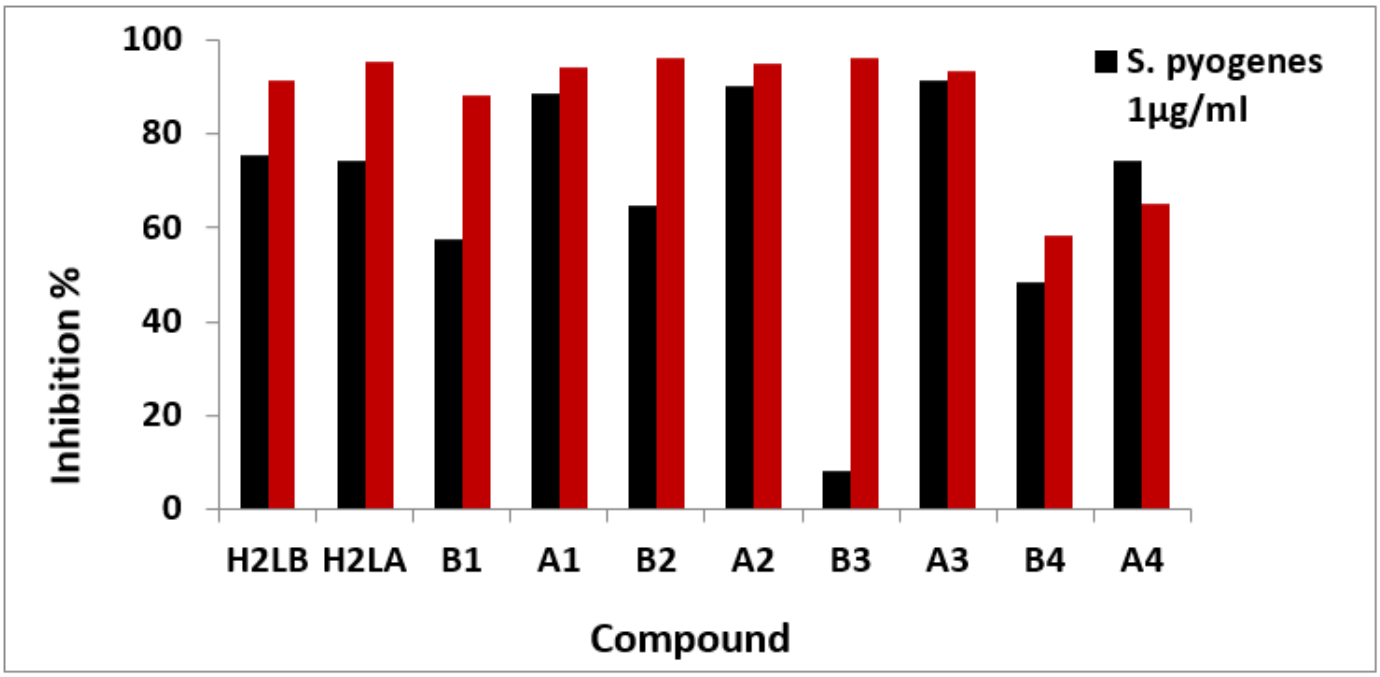

Figure 24

Antibacterial activity for ligand and copper, zinc and cadium (B1, B2,B3, B4 and A1,A2,A3, A4) complexes before and after irradiation against S. pyogenes

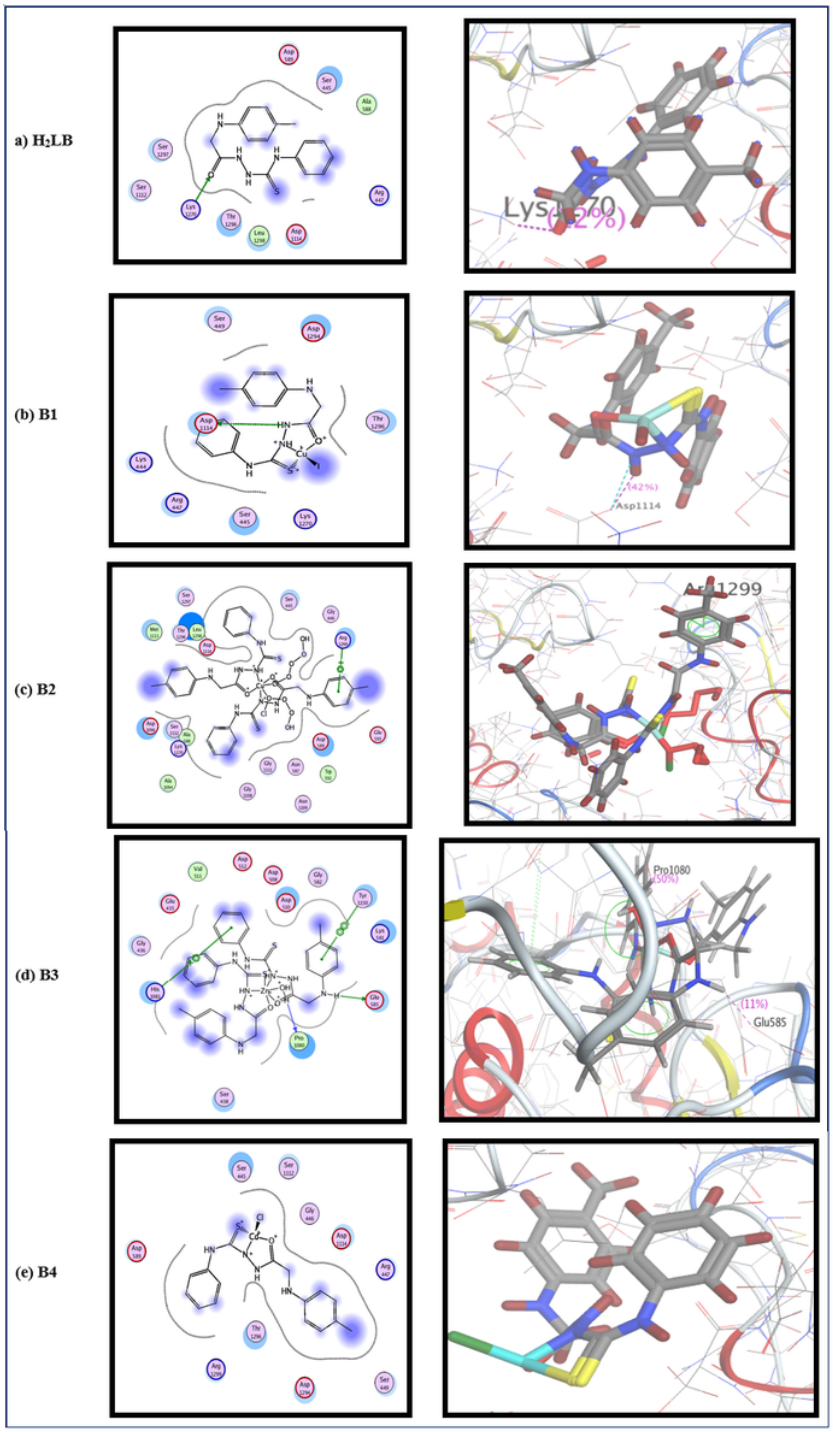

Figure 25

Binding pose of a) H2LB, b) [Cu(H2L)I], c) [Cu(H2L)2(ClO4)2],d) [Zn (H2L)2(H2O)]SO4 and e) [Cd(H2L)Cl]Cl complexes in the active pocket of topoisomerase II DNA gyrase enzymes (PDB ID: 2XCT).